ELSEVIER

Marine Geology 182 (2002) 351–372

MARINE GEOLOGY
INTERNATIONAL JOURNAL OF MARINE GEOLOGY, GEOCHEMISTRY AND GEOPHYSICS

www.elsevier.com/locate/margeo

Glacial–interglacial cycles in Sr and Nd isotopic composition of Arctic marine sediments triggered by the Svalbard/Barents Sea ice sheet

Thomas Tütken [a,*], Anton Eisenhauer [b], Bettina Wiegand [c], Bent T. Hansen [d]

[a] *Institut für Mineralogie, Petrologie und Geochemie, Universität Tübingen, Wilhelmstrasse 56, 72074 Tübingen, Germany*
[b] *GEOMAR, Forschungszentrum für marine Geowissenschaften, Wischofstrasse 1–3, 24148 Kiel, Germany*
[c] *Geochemisches Institut, Universität Göttingen, Goldschmidt Strasse 1, 37077 Göttingen, Germany*
[d] *IGDL, Institut für Geologie und Dynamik der Lithosphäre, Goldschmidt Strasse 3, 37077 Göttingen, Germany*

Received 24 July 2000; accepted 3 September 2001

Abstract

Sr and Nd isotopic compositions of Arctic marine sediments characterize changes of sediment source regions and trace shelf–ocean particle pathways during glacial–interglacial transitions in the eastern Arctic Ocean. In the 140-ka sedimentary record of a marine core from Yermak Plateau, north of Svalbard, $^{87}Sr/^{86}Sr$ ratios and ε_{Nd} values vary between 0.717 and 0.740 and −9.3 and −14.9, respectively. Sr and Nd isotopic composition both change characteristically during glacial–interglacial cycles and are correlated with the extension of the Svalbard/Barents Sea ice sheet (SBIS). The downcore variation in Sr and Nd isotopic composition indicates climatically induced changes in sediment provenance from two isotopically distinct end-members: (1) Eurasian shelf sediments as a distal source; and (2) Svalbard bedrock as a proximal source that coincide with a change in transport mechanism from sea ice to glacial ice. During glacier advance from Svalbard and intensified glacial bedrock erosion, ε_{Nd} values decrease gradually to a minimum value of −14.9 due to increased input of crystalline Svalbard bedrock material. During glacial maxima, the SBIS covered the entire Barents Sea shelf and supplied increasing amounts of Eurasian shelf material to the Arctic Ocean as ice rafted detritus (IRD). ε_{Nd} values in glacial sediments reach maximum values that are comparable to the average value of modern Eurasian shelf and sea ice sediments ($\varepsilon_{Nd} = -10.3$). This confirms ice rafting as a major sediment transport mechanism for Eurasian shelf sediments into the Arctic Ocean and trace a sediment origin from the Kara Sea/Laptev Sea shelf area. After the decay of the shelf-based SBIS, the glacial shelf sediment spikes during glacial terminations I ($\varepsilon_{Nd} = -10.6$) and II ($\varepsilon_{Nd} = -10.1$) ε_{Nd} values rapidly decrease to values of −12.5 typical for interglacial averages. The downcore Sr isotopic composition is anticorrelated to the Nd isotopic composition, but may be also influenced by grain-size effects. In contrast, the Nd isotopic composition in clay- to silt-size fractions of one bulk sediment sample is similar to within 0.3–0.8 ε_{Nd} units and seems to be a grain-size independent provenance tracer.

Keywords: strontium; neodymium; isotopes; Arctic Ocean; provenance; Svalbard/Barents Sea ice sheet

* Corresponding author.
E-mail address: thomas.tuetken@uni-tuebingen.de (T. Tütken).

0025-3227/02/$ – see front matter
PII: S0025-3227(01)00248-1

1. Introduction

The Arctic Ocean influences the global climate through its heat budget and has played an important role in Cenozoic climate evolution (e.g., Aagaard and Carmack, 1994; Alley, 1995). The extensive perennial sea ice cover of the Arctic Ocean is especially important in controlling heat flow, water circulation, bottom water formation, surface water productivity, and the sedimentation regime (e.g., Aagaard and Carmack, 1989; Clark, 1990; Anderson et al., 1994). High-resolution analyses of Arctic marine sediments potentially archive the history of northern hemisphere ice sheets, sea ice coverage, and surface water productivity triggered by changes in oceanic and atmospheric circulation patterns, continental glaciation and sea level (e.g., Stein et al., 1994a; Elverhøi et al., 1995; Lloyd et al., 1996; Spielhagen et al., 1997; Mangerud et al., 1998; Nørgaard-Pedersen et al., 1998; Knies et al., 1999, 2000; Vogt et al., 2001).

To constrain provenance of Cenozoic Arctic marine sediments and trace shelf–ocean particle pathways of river discharge, sea ice, and icebergs, detailed studies of lithology, bulk mineralogy, and stable isotopes of marine sediments were made (e.g., Stein et al., 1994b; Spielhagen et al., 1997; Vogt, 1997) including ice rafted debris (IRD) (Bischof et al., 1990, 1996; Spielhagen, 1991; Letzig, 1995; Nørgaard-Pedersen et al., 1998), clay mineralogy (Stein et al., 1994a; Wahsner et al., 1999), heavy mineral associations (Behrends et al., 1999) and organic geochemistry (Schubert and Stein, 1996; Fahl and Stein, 1999).

To obtain information on sediment sources and constrain transport processes of detrital Arctic Ocean sediments, $^{87}Sr/^{86}Sr$ and $^{143}Nd/^{144}Nd$ ratios were analyzed (Winter et al., 1997; Rachold et al., 1998; Eisenhauer et al., 1999). Sr and Nd isotopic ratios are suitable tracers for provenance studies of continental detritus (Goldstein and O'Nions, 1981; Goldstein et al., 1984; Goldstein and Jacobsen, 1988; Grousset et al., 1988; Revel et al., 1996a,b; Winter et al., 1997). They allow the reconstruction of oceanic and atmospheric circulation patterns (Asahara et al., 1995; Revel et al., 1996a,b; Fagel et al., 1999; Innocent et al., 1997) as well as particle pathways and sediment transport mechanisms (Grousset et al., 1988, 1992; Revel et al., 1996b; Hemming et al., 1998; Weis et al., 1997; Innocent et al., 2000; Walter et al., 2000).

In this study we use Sr and Nd isotope analyses to determine changes in provenance of marine sediments from a piston core in the eastern Arctic Ocean, NE of Svalbard, covering marine isotope stage (MIS) 6 to 1 (about 140 ka). The downcore isotope analysis can place constraints on climatically triggered changes in sediment provenance that are coupled to the build-up and decay of the Svalbard/Barents Sea ice sheet (SBIS), during glacial–interglacial climate cycles and the glacial erosion of different crustal rocks. These analyses will be compared with the Sr and Nd isotope composition of modern Eurasian shelf sediments and sediment-laden sea ice as well as other potential circum-Arctic sources.

2. Sediment transport processes in the modern eastern Arctic Ocean

The modern Arctic Ocean is a deep ocean basin surrounded by the vast continental masses of Siberia, North America, and Greenland (Fig. 1a). Deep-water exchange occurs only via the Fram Strait to the Atlantic Ocean, while surface water flows in through the Bering Strait, over the Barents shelf and through the Fram Strait as the warm West Spitsbergen Current. Nearly half of the Arctic Ocean surface area is underlain by continental shelves extending up to 800 km from the shoreline. The Eurasian shelf regions of Barents, Kara, Laptev, East Siberian and Chukchi Seas (Fig. 1a) are commonly very shallow (<30 m) and provide depositional environments for about 90% of the fluvial suspended particulate matter (SPM) delivered mainly by the Siberian rivers Yenisey, Lena, Ob, Kolyma and Khatanga (Milliman and Meade, 1983). Of the east Siberian rivers, the Lena with a 2.5 million km^2 drainage area, has the greatest runoff (525 km^3 a^{-1} and supplies most of the SPM (21×10^6 t a^{-1}) to the Laptev Sea, mainly during spring/summer runoff peaks (Gordeev et al., 1996). The similarity be-

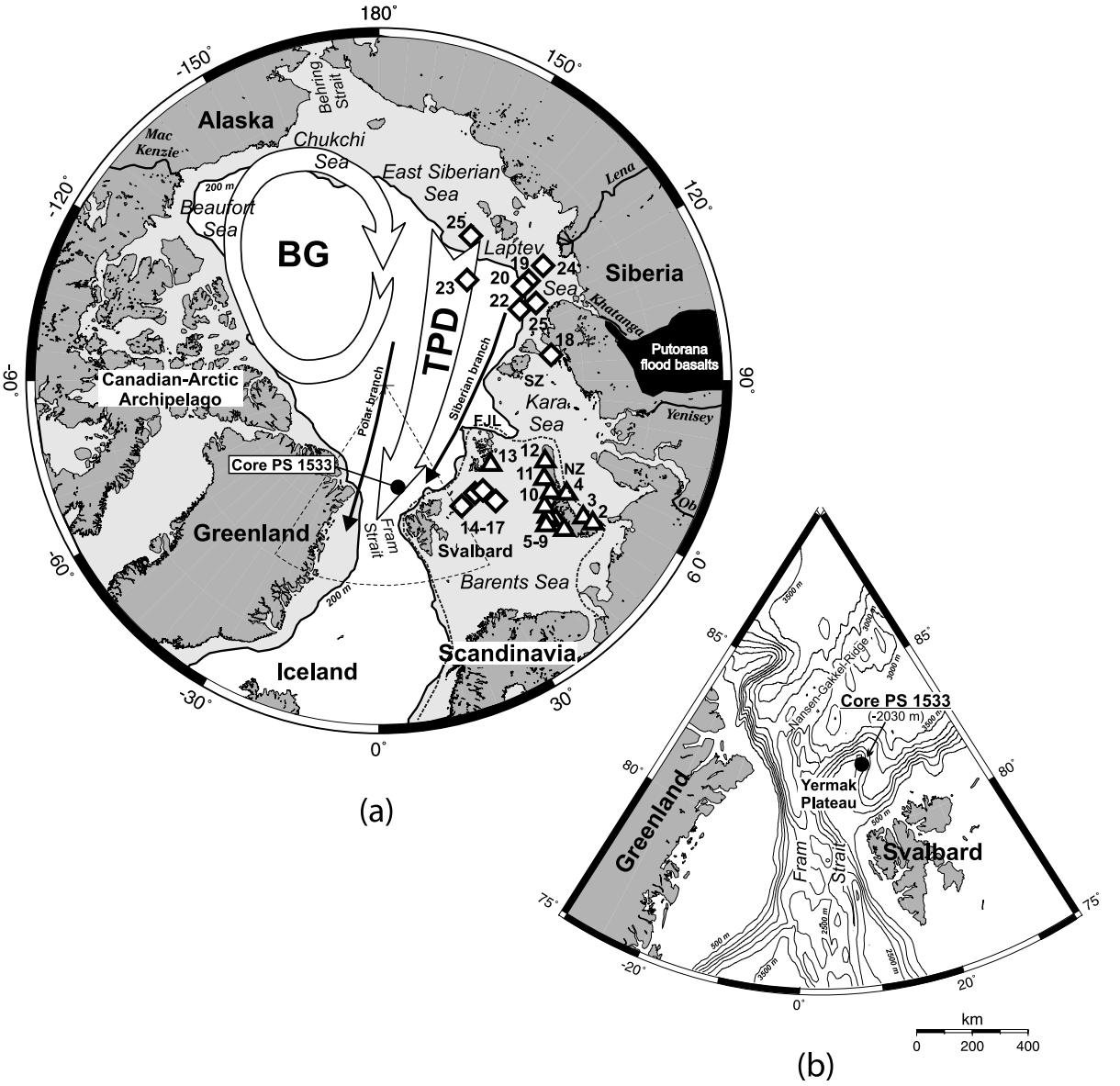

Fig. 1. (a) Map of sample locations in the Arctic Ocean with general surface circulation patterns (TPD = Transpolar Drift, BG = Beaufort Gyre) after Gordienko and Laktionov (1969). Sample numbers are according to Table 1. ● = sediment core PS1533, ◇ = sea ice sample, △ = shelf surface sediment, black area: Permo-Triassic Putorana flood basalts, FJL = Franz Josef Land, NZ = Novaya Zemlya, SZ = Svernaya Zemlya. Dotted line = maximum Eurasian ice sheet extension onto the Barents Sea shelf after Forman et al. (1999) and Lambeck (1995). (b) Bathymetric map of the location of core PS1533 on the Yermak Plateau, north of Svalbard.

tween Sr isotopic compositions of Lena river SPM, Laptev Sea shelf sediments, sediment laden sea ice and Arctic Ocean surface sediments provides evidence for the dispersion of riverine input by the Transpolar Drift from the Siberian hinterland across the Eurasian shelf into the Arctic Ocean (Rachold et al., 1998; Eisenhauer et al., 1999).

Table 1
Sample locations and Rb, Sr, and Nd concentrations and isotopic ratios of shelf and sea ice sediments

Sample	Sample location	Sample type	Depth (m)	Latitude	Longitude	Sr (ppm)	Rb (ppm)	$^{87}Rb/^{86}Sr$	$^{87}Sr/^{86}Sr \pm 2\sigma$	Nd (ppm)	$^{143}Nd/^{144}Nd \pm 2\sigma$	$\varepsilon_{Nd}^{(0)}$
1-1 to 1-34	Yermak Plateau	sediment core	2030	82°01′54″N	15°10′42″E	124*	117*	3.07*	0.72802*	29*	0.512002*	−12.5*
Barents Sea shelf												
2 (St. 5)	Abrosimov Fjord (NZ)	surface sediment	10	71°56′37″N	55°19′20″E	90	n.d.	n.d.	0.712860 ± 8	16	0.512432 ± 8	−4.0
3 (Step. 15)	Stepovogo Fjord (NZ)	surface sediment	36	72°32′60″N	55°29′35″E	62	97	4.5	0.725795 ± 9	17	0.512339 ± 8	−5.8
4 (St. 2)	Tsivolky Fjord (NZ)	surface sediment	30	74°26′13″N	58°37′24″E	76	115	4.35	0.731129 ± 15	23	0.512267 ± 8	−7.2
5 (1149)	Barents Sea (NZ)	surface sediment	63	73°10′50″N	52°20′00″E	210	54	0.74	0.714073 ± 13	13	0.511997 ± 8	−12.5
6 (1151)	Barents Sea (NZ)	surface sediment	65	73°30′00″N	52°50′00″E	187	52	0.8	0.713130 ± 16	20	0.511920 ± 8	−14.0
7 (1152)	Barents Sea (NZ)	surface sediment	152	74°00′00″N	53°00′00″E	138	83	1.73	0.717730 ± 16	18	0.512107 ± 8	−10.4
8 (1153)	Barents Sea (NZ)	surface sediment	132	74°00′00″N	53°32′00″E	170	53	0.9	0.713431 ± 8	18	0.512096 ± 7	−10.6
9 (1154)	Barents Sea (NZ)	surface sediment	144	74°30′00″N	54°40′00″E	127	n.d.	n.d.	0.716617 ± 9	23	0.512173 ± 7	−9.1
10 (200811)	Novaya Zemlya	surface sediment	53	75°59′10″N	57°98′30″E	96	141	4.25	0.733329 ± 13	30	0.512180 ± 7	−8.9
11 (200822)	Novaya Zemlya	surface sediment	53	76°25′39″N	61°23′72″E	92	n.d.	n.d.	0.730455 ± 8	26	0.512182 ± 8	−8.9
12 (200831)	Novaya Zemlya	surface sediment	150	76°47′50″N	6°51′96″E	169	95	1.62	0.716309 ± 9	19	0.512455 ± 9	−3.6
13 (280811)	Franz Josef Land	surface sediment	49	80°33′20″N	52°83′30″E	101	87	2.47	0.718640 ± 9	16	0.512151 ± 8	−9.5
Laptev Sea/Barents Sea												
14 (ARK 2241)	Barents Sea	sea ice sediment	surface	ca. 81°N	ca. 31°E	163	92	1.62	0.713129 ± 14	21	0.512215 ± 12	−8.3
15 (ARK 2281)	Barents Sea	sea ice sediment	surface	ca. 82.5°N	ca. 38°E	124	103	2.39	0.714886 ± 10	20	0.512155 ± 9	−9.4
16 (ARK 2291)	Barents Sea	sea ice sediment	surface	ca. 82.5°N	ca. 39°E	133	101	2.19	0.714894 ± 9	23	0.512191 ± 8	−8.7
17 (ARK 2331)	Barents Sea	sea ice sediment	surface	ca. 82°N	ca. 42°E	142	100	2.04	0.713991 ± 11	18	0.512199 ± 9	−8.6
18 (ARK 2401)	Kara Sea	sea ice sediment	surface	ca. 77.8°N	ca. 101°E	118	104	2.53	0.715311 ± 10	20	0.512183 ± 12	−8.9
19 (ARK 2512)	East Laptev Sea	sea ice sediment	surface	ca. 77.5°N	ca. 125°E	183	83	1.31	0.713602 ± 11	22	0.512042 ± 9	−11.6

Table 1 (*Continued*).

Sample	Sample location	Sample type	Depth (m)	Latitude	Longitude	Sr (ppm)	Rb (ppm)	$^{87}Rb/^{86}Sr$	$^{87}Sr/^{86}Sr \pm 2\sigma$	Nd (ppm)	$^{143}Nd/^{144}Nd \pm 2\sigma$	$\varepsilon_{Nd}^{(0)}$
20 (ARK 2531)	West Laptev Sea	sea ice sediment	surface	ca. 77.7°N	ca. 125°E	142	85	1.73	0.713940 ± 10	22	0.512173 ± 9	−9.1
21 (ARK 2581)	West Laptev Sea	sea ice sediment	surface	ca. 78.4°N	ca. 118°E	129	97	2.16	0.714521 ± 13	22	0.512199 ± 14	−8.6
22 (ARK 2621)	West Laptev Sea	sea ice sediment	surface	ca. 77.5°N	ca. 116°E	123	95	2.23	0.714631 ± 12	22	0.512160 ± 9	−9.3
23 (1111)	East Laptev Sea	sea ice sediment	ice core	ca. 79°N	ca. 140°E	139	n.d.	n.d.	0.718897 ± 9	30	0.512007 ± 9	−12.3
24 (1131)	East Laptev Sea	sea ice sediment	surface	ca. 75.5°N	ca. 131.5°E	221	n.d.	n.d.	0.714737 ± 9	27	0.511950 ± 8	−13.4
25 (1141-7)	East Laptev Sea	sea ice sediment	ice core	ca. 77°N	ca. 149°E	155	n.d.	n.d.	0.717450 ± 9	124	0.512034 ± 8	−11.8

Shelf surface samples are from the upper 1–2 cm of sediment. Sediment samples from sea ice are molten out and filtered off the solution. In-run uncertainties given for Sr and Nd isotope ratios are 2σ errors. ε_{Nd} are calculated as $\varepsilon_{Nd} = [[^{143}Nd/^{144}Nd_{sample} \ ^{143}Nd/^{144}Nd_{CHUR}] - 1] \times 10^4$ using the present-day CHUR value $^{143}Nd/^{144}Nd_{CHUR} = 0.512638$ (Jacobsen and Wasserburg, 1980).

* = mean value of core PS1533 sediments.

Fluvial input is the most important transport mechanism for sediment and fresh water supply via the Siberian shelf areas to the Arctic Ocean. The river discharge of fresh water into the Arctic Ocean produces a low salinity surface layer that promotes thermohaline stratification of the Arctic water masses and the formation of sea ice (e.g., Aagaard and Carmack, 1989; Spielhagen and Erlenkeuser, 1994). Sea ice accounts for ca. 99% of modern perennial central Arctic Ocean ice cover, while icebergs from glaciated continental areas (today: Ellesmere Island, Greenland, Svalbard, Svernaya Zemlya and Novaya Zemlya) contribute only about 1% (Clark, 1990).

In the Arctic Ocean, ice rafting plays a key role for shelf–ocean sediment transport and large amounts of fine-grained sediment are supplied to the central Arctic Ocean by ice rafting (Clark, 1990; Nürnberg et al., 1994; Reimnitz et al., 1994). Resuspended shelf sediments are incorporated into the newly formed sea ice by suspension freezing on shallow shelf regions with < 30 m water depth, especially in the Laptev Sea (Nürnberg et al., 1994; Reimnitz et al., 1994; Eicken et al., 1997). Sea ice export from the Laptev Sea with the highest net-ice production of ca. 400 $km^3\ a^{-1}$ (Eicken et al., 1997) is of major importance and delivers 3–4 million tons of shelf sediment to the Arctic Ocean by sea ice rafting during the winter season.

General pathways of sea ice motion are well known by drift research and buoy data (Colony and Thorndyke, 1985; Pfirman et al., 1997). Two major current systems dominate the modern surface water circulation in the Arctic Ocean: the anticyclonic Beaufort Gyre over the Amerasian Basin and various branches (Polar, Central and Siberian branches) of the south-west trending Transpolar Drift (TPD) over the Eurasian Basin (Gordienko and Laktionov, 1969) (Fig. 1a). The TPD transports newly formed sea ice from the Siberian shelf areas via the central Arctic Ocean to the Fram Strait within 2–3 years (Colony and Thorndyke, 1985) where it finally melts releasing most of its debris in the ablation area of the sea ice margin (Hebbeln and Wefer, 1991; Pfirman et al., 1997). Hence, most of the central Arctic Ocean sediments were derived from the continen-

tal shelf areas by sea ice rafting (e.g., Berner and Wefer, 1990; Clark, 1990). In glacial periods, ice rafting of icebergs from surrounding Eurasian ice sheets, especially the SBIS, contributed great amounts of IRD to the marine sedimentary record at the Svalbard Margin (Lloyd et al., 1996; Mangerud et al., 1998; Knies et al., 1999).

3. Materials and methods

The marine Arctic piston core PS1533, analyzed in this study, was raised on Polarstern expedition ARK IV/3 1987 at the Svalbard/Barents Sea Margin. Core location is on the Yermak Plateau north of Svalbard in 2030 m water depth (Fig. 1a,b, Table 1). In core PS1533 sediments are predominantly silty clays to clayey silts with sporadic dropstones and clay clasts. In glacial stage sediments the content of the >63 μm coarse fraction reaches up to 30 wt% and, owing to a higher input of IRD, the sedimentation rate exceeds the average rate of 3.1 cm ka^{-1} (Eisenhauer et al., 1994). Due to missing foraminiferas in core intervals with carbonate dissolution the age model of core PS1533 sediments was established on the basis of ^{10}Be-stratigraphy (Eisenhauer et al., 1994) and the SPECMAP time scale (Imbrie et al., 1984). The core represents a continuous sedimentary record of the last 140 ka, from marine isotope stage (MIS) 1–6. $^{87}Sr/^{86}Sr$ and $^{143}Nd/^{144}Nd$ ratios were measured on 34 core samples, covering these six MIS (Table 3). All Sr and Nd isotope analyses were made on the <63 μm grain-size fraction.

In order to estimate possible grain-size effects on the Rb–Sr and Sm–Nd isotope systematics, grain-size separates of two core sediment samples (1-4 and 1-17) were made by gravimetric settling, and analyzed for their isotopic compositions and concentrations of Rb, Sr, Sm, and Nd (Table 2). Sr and Nd isotope analyses of 24 modern Eurasian shelf and sea ice sediment samples were made to characterize potential Eurasian source regions (Table 1). The 12 surface sediment samples from Eurasian shelf areas were taken in 1991–1993 during several Russian and Norwegian Arctic expeditions to the Eurasian continental margin: six samples from fjords and shelf sites of Novaya Zemlya, five samples from the Barents shelf west of Novaya Zemlya and one from Franz Josef Land (Fig. 1a). The 12 samples of sediment-laden sea ice from Eurasian shelf areas were collected on the ESARE-expedition in 1992 and the ARK IX/4-expedition in 1993: four samples are from the Barents Sea, one is from the Kara Sea and seven are from the Laptev Sea. Exact sample locations and water depths are given in Table 1 and shown in Fig. 1a,b.

All <63 μm sediment samples were leached

Table 2
Rb, Sr and Sm, Nd concentrations and isotopic ratios of grain size fractions of two samples of core PS1533

	wt.%	Rb (ppm)	Sr (ppm)	$^{87}Rb/^{86}Sr$	$^{87}Sr/^{86}Sr \pm 2\sigma$	Sm (ppm)	Nd (ppm)	$^{147}Sm/^{144}Nd$	$^{143}Nd/^{144}Nd \pm 2\sigma$	$\varepsilon_{Nd}^{(0)}$	T_{DM}^{Nd} (Ga)
Sample 1-4											
<63 μm	97.0*	119	105	3.26	0.724732 ± 14	n.d.	29.5	n.d.	0.512041 ± 5	−11.7	n.d.
20–63 μm	7.1	55	226	0.97	0.713879 ± 11	3.25	17.9	0.1101	0.512069 ± 8	−11.1	1.58
2–20 μm	50.5	106	165	2.57	0.719669 ± 12	4.42	25.2	0.1060	0.512043 ± 10	−11.6	1.56
<2 μm	39.4	143	97	5.88	0.730086 ± 10	4.34	25.9	0.1014	0.512028 ± 10	−11.9	1.51
Sample 1-17											
<63 μm	99.4*	130	113	3.32	0.728261 ± 11	n.d.	33.0	n.d.	0.511994 ± 6	−12.6	n.d.
20–63 μm	6.8	58	151	1.52	0.719481 ± 11	3.62	20.4	0.1074	0.511971 ± 8	−13.0	1.68
2–20 μm	49.4	116	145	3.20	0.724219 ± 10	4.52	26.6	0.1027	0.511972 ± 7	−13.0	1.61
<2 μm	43.2	128	104	4.94	0.732102 ± 10	4.52	27.6	0.0989	0.511989 ± 7	−12.7	1.54

Grain-size separates were made by gravimetric settling in Atterberg tubes. Rb, Sr, Nd, and Sm concentrations were measured by isotope dilution technique. Nd model ages (T_{DM}) are calculated as $T_{DM} = (1/\lambda)\ln\{[(^{143}Nd/^{144}Nd)_{sample} - (^{143}Nd/^{144}Nd)_{DM}]/[^{147}Sm/^{144}Nd)_{sample} - (^{147}Sm/^{144}Nd)_{DM}]\}$ using present day depleted mantle values of Goldstein et al. (1984): $(^{143}Nd/^{144}Nd)_{DM} = 0.513151$ and $(^{147}Sm/^{144}Nd)_{DM} = 0.21378$. * = the difference to 100 wt.% is the grain-size fraction >63 μm.

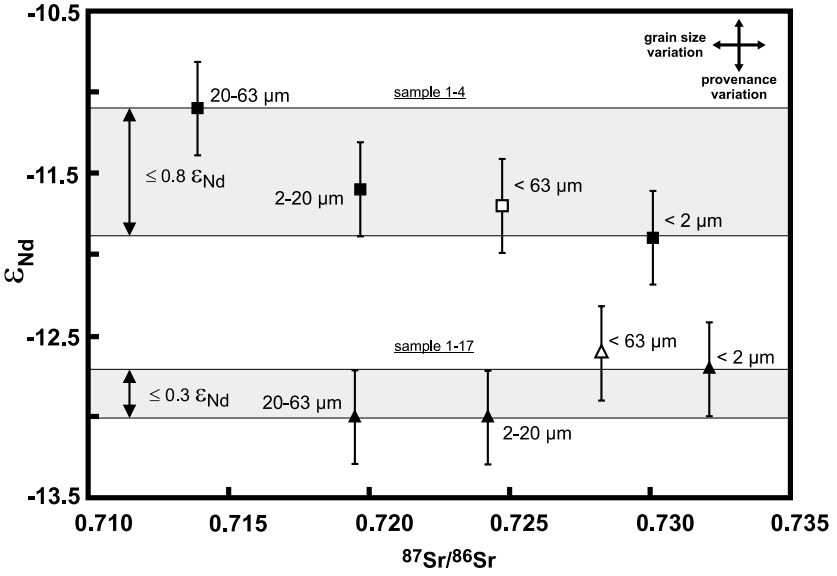

Fig. 2. ε_{Nd} versus $^{87}Sr/^{86}Sr$ diagram of the clay, fine silt, coarse silt (filled symbols) and <63 μm (open symbols) grain-size fractions of two sediments from core PS1533. square = sample 1-4 ($\sim$15 ka, MIS 2), triangle = sample 1-17 ($\sim$71 ka, MIS 5). Error bars are 2 S.D.$_{ext}$ external Nd standard reproducibility ($\pm$0.33 ε_{Nd}-units) which is in the same range as sample reproducibility. Gray shaded bars are the within sample variability of the ε_{Nd} values between the grain-size fractions of each sample, indicating the possible grain-size effect.

with suprapure 1.3 N HCl at room temperature for 1 h according to Asahara et al. (1995) and Eisenhauer et al. (1999) remove Sr-containing, authigenic marine mineral phases (e.g., biogenic carbonates and Fe/Mn oxy-hydroxides). Excess acid was removed by repeated washing with ultrapure water. This treatment removes sea water Sr (leachates: $^{87}Sr/^{86}Sr = 0.70913$–$0.70933$) that would obscure the detrital Sr isotope provenance signal. A 100-mg sample of the leached, de-carbonated sediment was dissolved at 190°C using a $HF–HNO_3–HClO_4$ mixture in PTFE beakers. To obtain Sr and Nd concentrations, samples were analyzed by isotope dilution technique using a mixed $^{87}Rb–^{84}Sr$ and $^{149}Sm–^{150}Nd$ spike added before sample dissolution. Sr and Nd fractions were separated by cation exchange chromatography.

Sr and Nd were loaded on Ta-single and Re-double filaments, respectively, and isotopic ratios were measured in static mode on a Finnigan MAT 262 RPQ$^+$ multicollector mass spectrometer. Equipment reproducibility was determined by measurement of the NBS-987 and La Jolla standards which gave average values of $^{87}Sr/^{86}Sr = 0.710249 \pm 33$ (2 S.D.$_{ext}$, $n = 14$) and $^{143}Nd/^{144}Nd = 0.511846 \pm 18$ (2 S.D.$_{ext}$, $n = 13$), respectively. All procedure blanks were negligible (Nd <200 pg and Sr <400 pg). Measured $^{87}Sr/^{86}Sr$ and $^{143}Nd/^{144}Nd$ ratios were corrected for mass fractionation by normalizing to $^{86}Sr/^{88}Sr = 0.1194$ and $^{146}Nd/^{144}Nd = 0.7219$, respectively, and for spike contributions. Rb concentrations of the <63 μm samples were measured by standard XRF procedures while Sr, Sm, and Nd concentrations were measured by isotope dilution technique. Uncertainties are $<6\%$ for Sr and Rb and $<0.5\%$ for Sm and Nd concentrations. To check reliability of results, duplicates where made of some samples (Table 3). Larger differences in Sr and Nd concentrations and isotopic compositions of some duplicates are probably due to grain-size effects because two aliquots of sample powder were taken from the same safe-lock vessel after centrifugation at the end of the leaching treatment. Sample inhomogeneity was further avoided by using the whole sample powder after centrifugation. Hence, the uncertainty of isotopic compo-

Table 3
Rb, Sr, and Nd concentrations and isotopic ratios for sediments of core PS1533

Sample	Depth (cm)	Age (ka)	Sr (ppm)	Rb (ppm)	$^{87}Rb/^{86}Sr$	$^{87}Sr/^{86}Sr \pm 2\sigma$	Nd (ppm)	$^{143}Nd/^{144}Nd \pm 2\sigma$	$\varepsilon_{Nd}^{(0)}$
Sediment core PS 1533									
1-1	7	2.5	149	105	2.03	0.722593 ± 10	27.7	0.512010 ± 6	−12.2
1-1 D	7		137	n.d.	n.d.	0.725012 ± 11	25.5	0.511992 ± 6	−12.6
1-2	23	8.6	121	114	2.72	0.725905 ± 11	28.8	0.511977 ± 6	−12.9
1-3	44	13.5	137	117	2.48	0.719998 ± 14	27.1	0.512113 ± 15	−10.2
1-3 D	44		134	n.d.	n.d.	0.719530 ± 13	26.1	0.512075 ± 6	−11.0
1-4	59	15.5	105	119	3.26	0.724732 ± 14	29.5	0.512041 ± 6	−11.7
1-5	70	17.2	108	133	3.26	0.735760 ± 11	30.8	0.511947 ± 9	−13.5
1-5 D	70		128	n.d.	n.d.	0.731440 ± 12	26.8	0.511936 ± 8	−13.7
1-6	83	18.6	108	111	2.96	0.724586 ± 11	30.8	0.512050 ± 5	−11.5
1-6 D	83		108	n.d.	n.d.	0.725564 ± 12	26.6	0.512061 ± 6	−11.2
1-7	99	20.8	104	131	3.63	0.736938 ± 10	27.4	0.511892 ± 4	−14.5
1-8	117	23.2	109	142	3.48	0.741186 ± 10	27.5	0.511877 ± 5	−14.9
1-8 D	117		119	n.d.	n.d.	0.740148 ± 13	31.7	0.511874 ± 8	−14.9
1-8 D	117		120	n.d.	n.d.	0.740081 ± 14	30.6	0.511870 ± 7	−15.0
1-9	137	29.3	114	135	3.42	0.733351 ± 11	25.9	0.511873 ± 6	−14.9
1-10	154	35.6	126	134	3.08	0.732555 ± 11	27.8	0.511900 ± 12	−14.4
1-11	182	45.1	103	115	3.23	0.730117 ± 10	28.6	0.511998 ± 5	−12.5
1-12	197	50.2	107	128	3.46	0.729820 ± 11	27.5	0.511976 ± 5	−12.9
1-13	223	58.6	115	126	3.17	0.724349 ± 12	31.7	0.512052 ± 7	−11.4
1-14	243	63.2	113	127	3.24	0.725116 ± 14	32.8	0.512060 ± 14	−11.3
1-15	264	67.8	108	128	3.41	0.726654 ± 10	33.0	0.512033 ± 6	−11.8
1-16	274	69.8	106	126	3.42	0.729863 ± 11	31.3	0.511994 ± 7	−12.6
1-17	278	71.3	113	130	3.32	0.728261 ± 11	33.0	0.511994 ± 6	−12.6
1-18	280	72.4	105	138	3.78	0.730891 ± 11	30.8	0.511995 ± 7	−12.6
1-19	294	78.5	127	129	3.02	0.727583 ± 10	23.7	0.511950 ± 7	−13.4
1-19 D	294		120	n.d.	n.d.	0.727610 ± 9	23.8	0.511949 ± 7	−13.4
1-19 D	294		123	n.d.	n.d.	0.728774 ± 11	n.d.	n.d.	n.d.
1-20	314	87.6	124	124	2.88	0.728501 ± 11	28.8	0.511954 ± 6	−13.3
1-21	334	96.6	130	119	2.65	0.727946 ± 10	28.7	0.511961 ± 7	−13.2
1-22	354	105.8	131	132	2.91	0.728279 ± 13	32.1	0.511998 ± 19	−12.5
1-23	374	114.8	125	131	3.01	0.727565 ± 14	30.3	0.511994 ± 7	−12.6
1-24	378	116.4	122	136	3.21	0.729114 ± 12	30.2	0.511994 ± 6	−12.6
1-25	384	119.4	132	141	3.14	0.726246 ± 10	25.4	0.511967 ± 5	−13.1
1-25 D	384		127	n.d.	n.d.	0.728182 ± 12	25.5	0.511961 ± 7	−13.2
1-26	388	120.9	126	136	3.11	0.727580 ± 16	29.5	0.511964 ± 11	−13.2
1-27	394	124.0	105	122	3.36	0.726498 ± 11	30.3	0.512000 ± 5	−12.4
1-28	398	125.3	110	115	3.02	0.728796 ± 11	29.9	0.511998 ± 5	−12.5
1-29	401	125.9	113	117	2.99	0.727383 ± 12	31.4	0.512013 ± 5	−12.2
1-30	406	127.1	124	119	2.77	0.727320 ± 12	28.6	0.511996 ± 9	−12.5
1-31	411	127.8	139	104	2.15	0.717276 ± 11	31.3	0.512119 ± 7	−10.1
1-32	441	133.5	99	105	3.07	0.724287 ± 10	28.6	0.512126 ± 7	−10.0
1-33	455	136.7	101	103	2.93	0.722031 ± 14	27.6	0.512163 ± 7	−9.3
1-34	473	140.3	132	118	2.93	0.731754 ± 15	30.7	0.511915 ± 6	−14.1
1-34 D	473		128	118	2.93	0.734228 ± 13	n.d.	n.d.	n.d.
Average value			124	117	3.07	0.72796 ± 1	29	0.512001 ± 7	−12.5

Sample ages are interpolated according to the age model based on Be-stratigraphy of core PS1533 sediments (Eisenhauer et al., 1994). In-run uncertainties given for Sr and Nd isotope ratios are 2σ errors. Sr and Nd concentrations were measured by isotope dilution, Rb was measured by XRF. D = duplicates, which are complete chemical and mass spectrometric procedures on different sample aliquots. ε_{Nd} values are calculated as $\varepsilon_{Nd} = [[^{143}Nd/^{144}Nd_{sample}/^{143}Nd/^{144}Nd_{CHUR}]-1]\times 10^4$ using the present-day CHUR value $^{143}Nd/^{144}Nd_{CHUR} = 0.512638$ (Jacobsen and Wasserburg, 1980).

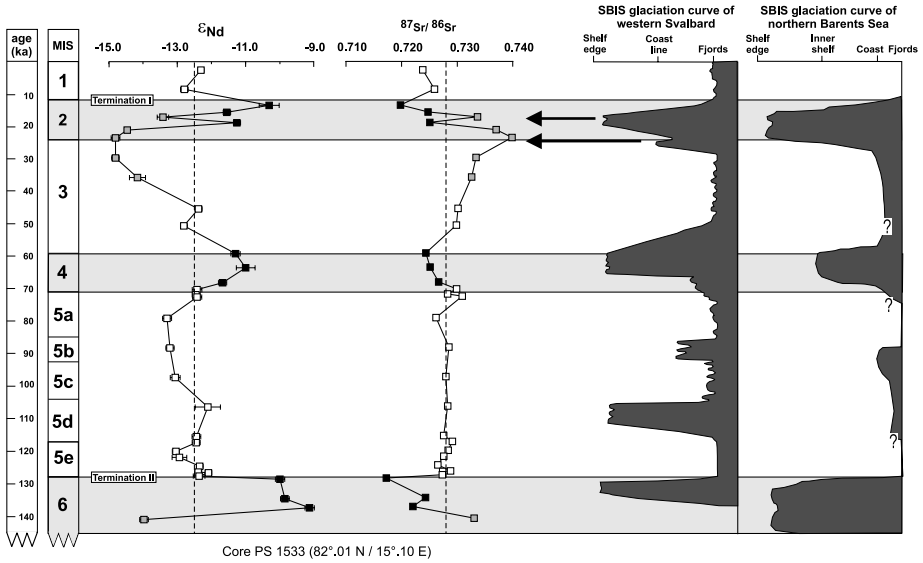

Fig. 3. Downcore variation in $^{87}Sr/^{86}Sr$ ratio and ε_{Nd} values of the <63-μm sediment fraction in core PS1533 over the last 140 ka. Gray shaded horizontal bands correspond to the glacial isotope stages. Black square = samples from glacial maxima and terminations with maximum Svalbart/Barents sea ice sheet extension onto the shelf and highest shelf sediment input; gray square = samples from SBIS build-up with highest input of Svalbard material; open square = samples from interglacial periods with average core sedimentation. Vertical dotted lines represent average isotopic values of the core sediments ($\varepsilon_{Nd} = -12.5$; $^{87}Sr/^{86}Sr = 0.728$). Error bars are 2σ; for the $^{87}Sr/^{86}Sr$ ratio they are smaller than symbol-size. SBIS glaciation curves of the northern Barents Sea shelf after Knies et al. (2000) and for western Svalbard after Mangerud et al. (1998). Downcore variation of Sr and Nd isotopic data of core PS1533 sediments correlates well with the SBIS glaciation curve of the northern Barents Sea, while glacier extensions of the western Svalbard glaciers in MIS 5d and 5b found by Mangerud et al. (1998) are not reflected in PS1533 sediments. But the two build-up phases of the SBIS in MIS 2 between 27 and 23 ka and 19 and 16 ka seem to be recorded in PS1533 sediments (black arrows).

sition and concentration increased significantly (sample 19 and 25, Table 3). According to duplicates, the true external reproducibility for $^{143}Nd/^{144}Nd$ ratios is $<0.002\%$, which corresponds to <0.2 ε_{Nd} units and is in the range of external reproducibility of ± 0.33 ε_{Nd} units.

4. Results

4.1. Relation of sediment particle-size and Rb–Sr and Sm–Nd isotope systematics

To estimate the $^{87}Sr/^{86}Sr$ and ε_{Nd} variations that may result from grain-size effects we analyzed the Rb–Sr and Sm–Nd isotopic compositions of three size fractions: <2, 2–20, and 20–63 μm from the two core samples 1-4 ($\sim$15 ka, MIS 2) and 1-17 ($\sim$71 ka, MIS 5) with similar grain-size distribution (Table 2). $^{87}Sr/^{86}Sr$ and $^{87}Rb/^{86}Sr$ ratios are inversely correlated with sediment particle-size and decrease, respectively, from 0.730 (<2 μm) to 0.714 (20–63 μm) and 5.88 to 0.97 in sample 1-4, and from 0.732 to 0.719 and 4.94 to 1.52 in sample 1-17 (Table 2). The magnitude of change in $^{87}Sr/^{86}Sr$ between the coarse silt and the clay fraction of one single sample (Fig. 2, Table 2) is similar to the range of all 34 core bulk samples (<63 μm) (Table 3). This grain-size influence on $^{87}Sr/^{86}Sr$ ratios must be considered when interpreting Sr-isotope compositions in terms of provenance and only well defined grain-size fractions should be compared.

In contrast, there is no significant dependence of Sm–Nd isotopic ratios on particle grain-size, because these elements seem not to be fractionated between mineralogically different grain-size fractions during the sedimentary cycle. With de-

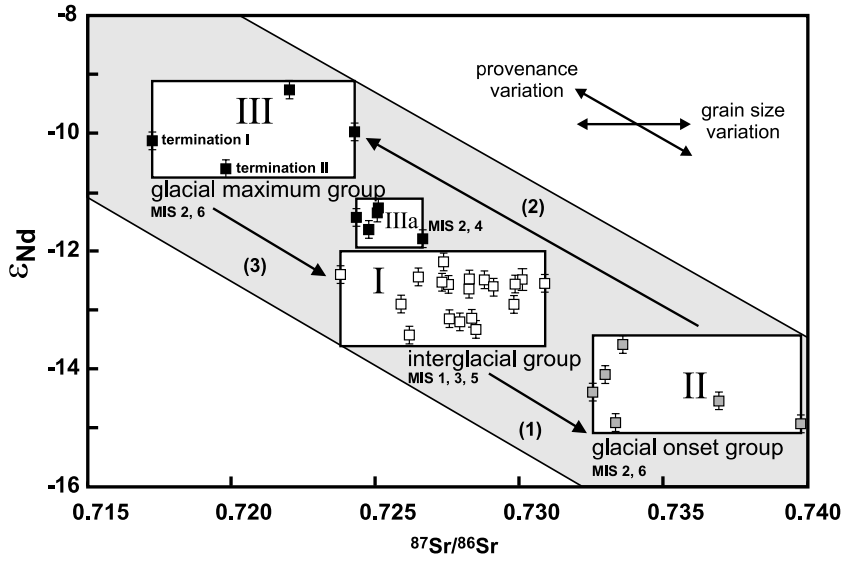

Fig. 4. ε_{Nd} versus $^{87}Sr/^{86}Sr$ diagram. Symbols are the same as in Fig. 3. The core samples are classified into three main groups according to their isotopic composition and marine isotope stages: interglacial group (I), glacial onset group (II) and glacial maximum group (III), (IIIa) is a subgroup of group (III). Arrows (1)–(3) mark the shift of Sr and Nd isotopic composition during the large glacial–interglacial cycles.

creasing grain-size ε_{Nd} values and $^{147}Sm/^{144}Nd$ ratios decrease from −11.1 to −11.9 and 0.1101 to 0.1014, respectively, in sample 1-4. Corresponding Nd-model age (T_{DM}) decreases from 1.58 to 1.51 Ga. In sample 1-17, ε_{Nd} values increase slightly with decreasing size fractions from −13.0 to −12.7, which is within analytical error (Fig. 2), while $^{147}Sm/^{144}Nd$ ratios decrease from 0.1074 to 0.0989. The corresponding T_{DM} decreases from 1.68 to 1.54 Ga (Table 2).

4.2. Temporal variations of Sr and Nd isotopic composition in core PS1533

The Sr and Nd isotopic compositions of the core sediments are reported in Table 3. $^{87}Sr/^{86}Sr$ and ε_{Nd} values show a temporal variation over a wide range from 0.717 to 0.740 and −9.3 to −14.1, averaging 0.728 and −12.5, respectively (Fig. 3). Core ε_{Nd} values are inversely correlated with $^{87}Sr/^{86}Sr$ ratios (Fig. 3), and vary strongly during MIS 2 and 6 triggered by the growth and decay of the SBIS according to the glaciation curves of Mangerud et al. (1998) and Knies et al. (2000) (Fig. 3). Maximum extension of the Svalbard glaciers onto the Barents shelf is coupled with an increase of ε_{Nd} values and a decrease of $^{87}Sr/^{86}Sr$ ratios. Samples of MIS 4 show the same but weaker trend, reflecting smaller extension of SBIS compared to MIS 2 and 6. During interglacials MIS 1 and 5 and to lesser extent in MIS 3, $^{87}Sr/^{86}Sr$ ratios and ε_{Nd} values deviate only slightly from average values (Fig. 3, Table 3).

According to their isotopic composition and MIS, the core samples can be divided into three main groups (I–III) (Fig. 4). Interglacial group (I) contains all samples from interglacial periods (MIS 1, 3 and 5) with intermediate $^{87}Sr/^{86}Sr$ ratios (0.723 to 0.730) and ε_{Nd} values (−12.2 to −13.4). Glacial onset group (II) comprises samples from the beginning of glacial MIS 2 and 6 and one sample from upper MIS 3 with lower ε_{Nd} values (less than −13.5) and higher $^{87}Sr/^{86}Sr$ ratios (0.732 to 0.740) compared to interglacial samples of group I. Glacial maximum group (III) contains samples of the ultimate and penultimate glacial maximum of MIS 2 and 6, including termination I and II. These samples have the highest ε_{Nd} values (greater than −10.5) and the lowest $^{87}Sr/^{86}Sr$ ratios (0.717 to 0.724). Subgroup (IIIa) comprises

samples of MIS 4 and two samples of MIS 2 showing a similar but weaker trend towards higher ε_{Nd} values and lower $^{87}Sr/^{86}Sr$ ratios compared to group (III) samples (Fig. 4).

The Sr and Nd isotope record of the core sediments show large glacial–interglacial changes (Fig. 3) following a characteristic pattern between these groups (I–III) (Fig. 4). Such a glacial–interglacial cycle starts in the interglacial period (group I) around the core average values of $\varepsilon_{Nd} = -12.5$ and $^{87}Sr/^{86}Sr = 0.728$. Due to increasing input of less radiogenic Nd and more radiogenic Sr, ε_{Nd} values reached minimum values of -14.9 but maximum $^{87}Sr/^{86}Sr$ ratios of 0.740 (group II) at or shortly after the interglacial/glacial transition. Within glacial MIS 2 and 6, $^{87}Sr/^{86}Sr$ ratios decreased to lowest values of 0.719 and 0.717 and ε_{Nd} values increased to highest values of -10.6 and -10.1 in the glacial terminations I and II, respectively (group III). Data for the two core samples 1-3 ($\sim$13.5 ka) and 1-30 ($\sim$128.5 ka) of termination I and II, respectively, fall in the field of Eurasian shelf sediments (Fig. 5), indicating dominant input of Eurasian shelf material during the ultimate and penultimate deglaciation event of the SBIS. At glacial/interglacial boundaries MIS (2/1) and MIS (6/5e), after glacial termination I and II, core $^{87}Sr/^{86}Sr$ ratios abruptly increased and ε_{Nd} values decreased to interglacial average values (Fig. 3), indicating a return to an interglacial sedimentation regime (group I).

The downcore variations of ε_{Nd} values cannot be attributed to grain-size effects because the range of 4.8 ε_{Nd} units is much larger than possible grain-size effects (< 0.8 ε_{Nd} units, Fig. 2). The differences in ε_{Nd} values must, therefore, reflect changes in sediment provenance from isotopically distinct crustal sources between interglacial and glacial periods. Similar glacial–interglacial cycles of Sr and Nd isotopic composition due to changing provenance and transport mechanisms were observed in contemporaneous marine Antarctic

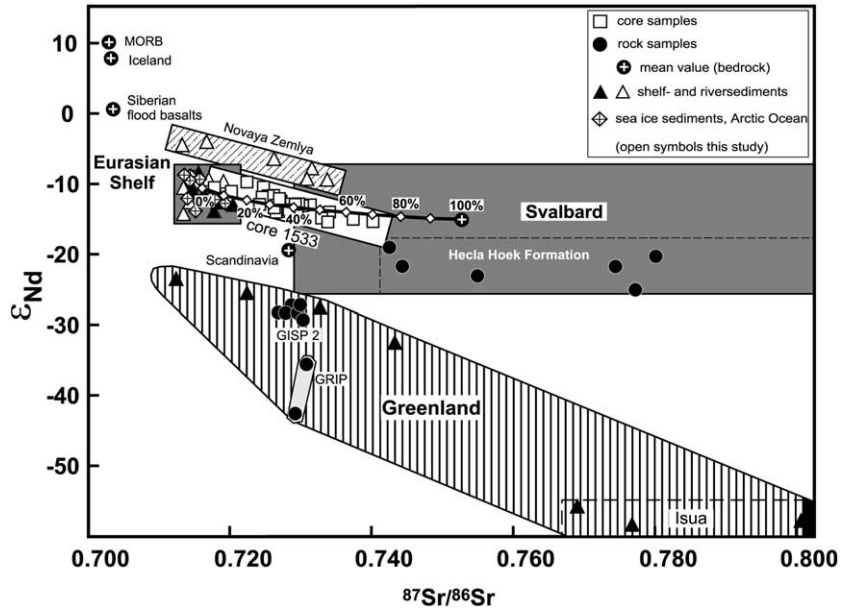

Fig. 5. ε_{Nd} versus $^{87}Sr/^{86}Sr$ diagram summarizing the isotope compositions of the core sediments in relation to whole rock, river, shelf and sea ice sediment samples covering the circum-Arctic region. Eurasian shelf sediment data are from this study and Eisenhauer et al. (1999); Svalbard data from Johansson et al. (1995, 2000) and Johansson and Gee (1999), Johansson (personal communication); Greenland data from McCulloch and Wasserburg (1978), Goldstein and Jacobsen (1988), and Weis et al. (1997); Scandinavian data from Miller et al. (1986), Novaya Zemlya data from this study, MORB data from Revel et al. (1996b), Iceland data from Revel et al. (1996b) and references therein, Siberian flood basalt data from Sharma et al. (1992) and Buechel (personal communication).

sediments (Walter et al., 2000) as well as on larger time scales in Arctic marine sediments by Winter et al. (1997).

4.3. Sr and Nd isotopic composition of modern Arctic shelf and sea ice sediments

The $^{87}Sr/^{86}Sr$ and ε_{Nd} values of all modern shelf and sea ice sediment samples are given in Table 1 and sample locations are shown in Fig. 1a. The 12 modern Eurasian shelf sediments from or near Novaya Zemlya vary over a wide range of 0.713 to 0.733 and −3.6 to −14.0, respectively. The three fjord samples (2, 3 and 4) of eastern Novaya Zemlya have $^{87}Sr/^{86}Sr$ ratios and ε_{Nd} values of 0.713 to 0.731 and −4.0 to −7.2, respectively. The five samples (5–9) from the shelf west of Novaya Zemlya have different isotopic compositions ($^{87}Sr/^{86}Sr = 0.713$ to 0.717; $\varepsilon_{Nd} = -9.1$ to −14.0) with much lower ε_{Nd} values similar to Eurasian shelf and sea ice samples. The other three Novaya Zemlya coastal samples (10–12) have an isotopic composition similar to those of the eastern fjord samples (Table 1). The isotopic composition of sample (13) from Franz Josef Land is similar to the isotopic composition of Eurasian shelf and sea ice sediments (Table 4).

Sediment-laden sea ice from the Eurasian shelf areas (Barents, Kara and Laptev Seas) supplying the Siberian branch of the TPD with sea ice has a narrow range of Sr and Nd isotopic composition ($^{87}Sr/^{86}Sr = 0.713$ to 0.715; $\varepsilon_{Nd} = -8.3$ to −9.4), except for samples 19, 23, 24, and 25 from the eastern Laptev Sea for which ε_{Nd} values are lower ($\varepsilon_{Nd} = -11.6$ to −13.4) and $^{87}Sr/^{86}Sr$ ratios are higher ($^{87}Sr/^{86}Sr = 0.719$ and 0.717; samples 23 and 25) (Table 1). Although geographically widespread, the sea ice samples have Sr and Nd isotopic compositions that are similar to those of their Eurasian shelf source regions (especially the Laptev Sea) (Table 4 and Fig. 5).

5. Discussion

5.1. Sr and Nd isotopic composition and sediment particle size

Grain-size effects on $^{87}Sr/^{86}Sr$ ratios of sediments due to varying mineralogical and hence chemical composition of different size fractions (Dasch, 1969; Goldstein et al., 1984; Douglas et al., 1995; Eisenhauer et al., 1999) are confirmed in this study. This phenomenon results in a large spread in $^{87}Rb/^{86}Sr$ and $^{87}Sr/^{86}Sr$ ratios between the different grain-size fractions (Fig. 2, Table 2),

Table 4
Average Sr and Nd concentration and isotopic composition of core PS1533 sediments, Svalbard bedrocks, and modern Arctic shelf and sea ice sediments

Sample type	Values	Sr (ppm)	$^{87}Sr/^{86}Sr$	Nd (ppm)	$\varepsilon_{Nd}^{(0)}$
Core 1533 sediment[a]	$n = 34$	124	0.72802	29	−12.5
Svalbard bedrock[b]	$n = 58$	132	0.75251	49	−14.6
Arctic Ocean sea ice[a]	$n = 12$	148	0.71495	23	−10.0
West Laptev Sea ice[a]	$n = 3$	131	0.71436	22	−9.0
West Laptev Sea shelf[c]	$n = 3$	168	0.71450	n.d.	−9.4
East Laptev Sea ice[a]	$n = 4$	174	0.71617	26	−12.3
East Laptev Sea shelf[c]	$n = 3$	158	0.71750	n.d.	−12.2
Barents Sea ice[a]	$n = 4$	140	0.71423	21	−8.7
Kara Sea ice[a]	$n = 1$	118	0.71531	20	−8.9
Novaya Zemlya fjords and shelf[a]	$n = 6$	97	0.72498	22	−6.4
Eurasian shelf sediments (+Arctic Ocean sea ice)[a,b]	$n = 31$	159	0.71585	21	−10.3

[a] Data from this study.
[b] Data from Johansson et al. (1995, 2000); Johansson and Gee (1999); Johansson, personal communication.
[c] Data from Eisenhauer et al. (1999). For ε_{Nd} and $^{87}Sr/^{86}Sr$ weighted average values have been calculated based on the relative concentration of Nd and Sr in the rocks.

although all size fractions probably come from the same source. $^{87}Sr/^{86}Sr$ ratios are only suitable to distinguish different sediment sources when data from the same grain-size fraction are compared.

In contrast, Sm and Nd seem not to be fractionated between mineralogically different silt and clay size fractions. Hence, the ε_{Nd} values of all three grain-size fractions (<2, 2–20, 20–63 μm) are almost identical in one sample (0.3 ε_{Nd} units in 1-17 and 8 ε_{Nd} units in 1-4) (Fig. 2). The grain-size fractions of each bulk sample all overlap within analytical error (Fig. 2), except the coarse silt fraction of sample 1-4 which has a higher ε_{Nd} value, probably indicating a different source compared to the fine fractions. This confirms that all three size fractions of each sample have a crustal source with similar Sm–Nd systematics and thus the same crustal residence times (T_{DM}) and ε_{Nd} values (McCulloch and Wasserburg, 1978; Goldstein and Jacobsen, 1988). Therefore, differences in Nd isotopic ratios in the sediments are caused by input from source regions with different Sm–Nd systematics. The difference in ε_{Nd} values (0.9 ε_{Nd} units) between the two bulk (<63 μm) samples 1-4 and 1-17 (Fig. 2, Table 2) is three times larger than analytical error (± 0.3 ε_{Nd} units) and, therefore, indicates a variation in sediment provenance between MIS 2 and MIS 5, respectively. This difference cannot be attributed to grain-size effects because these samples have very similar grain-size distributions (Table 2). Furthermore, the differences in ε_{Nd} between the same size fractions of these samples are 0.8–1.9, increasing from the clay to the coarse silt fraction (Fig. 2, Table 2). This supports a different source origin of all the size fractions of each sample. The increasing difference between the clay and silt fractions might be interpreted as a grain-size effect but may also be due to different sources of the size fractions. This has to be verified by sediment samples where all size fractions definitely come from the same crustal source to avoid different provenance of the grain-size fractions. Walter et al. (2000) found no significant differences between the Nd isotopic composition of the clay and silt fraction of a till sample, which supports the idea of grain-size-independent Nd isotopic composition.

The fact that both Sr and Nd isotopic compositions of the core sediments are changing in parallel (Fig. 3) must be related to variations in sediment provenance rather than to grain-size effects which would merely cause a change in Sr isotopic composition without significant changes in ε_{Nd} values. The Nd isotopic composition of grain-size separates can, therefore, provide more information about the sedimentary history than bulk samples and thus allow for a distinction of provenance and transport processes for different size fractions (McLennan et al., 1989; Revel et al., 1996a; Fagel et al., 1999; Innocent et al., 2000; Walter et al., 2000).

5.2. Potential sediment sources for the Arctic Ocean

5.2.1. Sr and Nd isotopic composition of circum Arctic crustal terranes

ε_{Nd} values and $^{87}Sr/^{86}Sr$ ratios of sediment samples and potential circum-Arctic source regions are graphically displayed in Fig. 5. In this diagram, data points for all samples of core PS1533 form an array between the two potential isotopic end-members: Eurasian shelf sediments (weighted average: $^{87}Sr/^{86}Sr = 0.71585$; $\varepsilon_{Nd} = -10.3$) and Svalbard bedrock (weighted average: $^{87}Sr/^{86}Sr = 0.75251$; $\varepsilon_{Nd} = -14.6$) (Table 4).

The Eurasian shelf end-member comprises shelf surface sediments and sea ice samples from the Barents, Kara and Laptev Seas (Fig. 1a). These fine-grained sediments have $^{87}Sr/^{86}Sr$ ratios of 0.713 to 0.719 and ε_{Nd} values ranging from -8.3 to -13.4 (Table 1). Sea ice samples of the Siberian branch of the TPD form a more restricted group within the shelf sediments with $^{87}Sr/^{86}Sr$ ratios of 0.713 to 0.715 and ε_{Nd} values of -8.3 to -9.4, which reflect their dominant western Laptev Sea origin. The average $^{87}Sr/^{86}Sr$ ratio of 0.716 and ε_{Nd} value of -10.3 for all Eurasian shelf and sea ice sediments (Table 4) are equivalent to average global river SPM with $^{87}Sr/^{86}Sr$ of 0.716 and ε_{Nd} of -10.6 (Goldstein and Jacobsen, 1988). Eurasian shelf sediments as natural mixed samples of the drained continental crust in the vast Siberian hinterland have a narrow range of Sr and Nd isotope composition

which is distinct from those of other source terranes like Greenland or Svalbard (Fig. 5), which partly consist of very old Precambrian crustal rocks. Therefore, the Svalbard Archipelago close to the core location is the most likely end-member for sediments with a high $^{87}Sr/^{86}Sr$ ratio and low ε_{Nd} value. Because there are no isotope data for sediments from Svalbard, whole rock Sr and Nd isotope data are used to characterize Svalbard as sedimentary source region.

The bedrock geology of Svalbard can be divided in three litho-tectonic sequences: post-Devonian sedimentary cover rocks, Devonian Old Red Sandstone sequences and pre-Devonian basement rocks of Palaeoproterozoic to Early Palaeozoic age that form three Caledonian terranes (e.g., Harland, 1985). The Lower Hecla Hoek Formation/Stubendorffbreen Supergroup/Atomfjella Complex in western Ny Friesland (Eastern Terrane) is a 15–20-km-thick metamorphic rock unit consisting of Palaeoproterozoic to Early Palaeozoic meta-sedimentary and meta-igneous rocks that form a tectonostratigraphic succession of alternating basement and cover units, thrusted, folded, and metamorphosed during the Caledonian orogeny (Gee et al., 1994). These Proterozoic crystalline basement rocks with U–Pb zircon ages of 1720–1780 Ma, have present-day $^{87}Sr/^{86}Sr$ ratios of 0.742 to 1.369 and present-day ε_{Nd} values of −18.6 to −24.6 (Johansson et al., 1995; Johansson and Gee, 1999). On Nordaustlandet (Eastern Terrane), a Grenville-age (~950 Ma) basement of meta-volcanic and granitic rocks is overlain by Neoproterozoic to Early Palaeozoic sediments and intruded by Caledonian (~420 Ma) granites (Gee et al., 1995; Johansson et al., 2000). The Grenvillian and Caledonian igneous rocks all have present-day ε_{Nd} values between −6.1 and −13.8 (Johansson et al., 2000). All these rocks outcrop in the northern areas of the Svalbard archipelago and are likely to represent the Svalbard end-member (Fig. 5). They are the most probable source for rock material with high $^{87}Sr/^{86}Sr$ ratios and low ε_{Nd} values eroded during Pleistocene glaciations of the Svalbard archipelago and supplied to the Svalbard Margin sediments. This is in agreement with the petrography of dropstones (metamorphic and magmatic rock fragments) of glacial MIS sediments in the Fram Strait (Bischof et al., 1990). Further evidence for an input of crystalline bedrock material of Svalbard origin by increased iceberg transport includes, high quartz and amphibole and reduced feldspar contents in IRD-rich MIS 2 sediments of neighboring core PS 2212-3 from Yermak Plateau (Vogt et al., 2001).

Siberia might have also contributed some crystalline IRD from glaciated areas in the region of the Kara/Barents Sea to Arctic Ocean sediments (Spielhagen et al., 1997). Contributions of Siberian material are also indicated by the presence of mature coal fragments originating from Siberian outcrops (Bischof et al., 1990). Siberia was partially glaciated during MIS 6, 4 and perhaps to a lesser extent in MIS 2 (Velichkov et al., 1997), but the glaciation is still in debate and was probably restricted on mountain areas, hence glaciers did not reach the shelf edge to contribute large amounts of IRD, therefore this source is not considered as important.

Contribution of material from the Amerasian and Greenland area is not likely because ε_{Nd} values of less than −20 are typical for these dominantly Precambrian rocks (Fig. 5). However, there are also some younger rocks of Phanerozoic age that crop out in the northeastern part of Greenland. Contribution of these rocks to the sedimentary record of core PS1533 is unlikely because IRD of the Svalbard Margin sediments contains no characteristic Amerasian rock material (Spielhagen, 1991; Kubisch, 1992) and Arctic Ocean surface circulation patterns (Fig. 1a) limit ice and sediment transport from the Amerasian Basin towards the Eurasian Margin.

Novaya Zemlya sediments show too high ε_{Nd} values and fall above the isotopic mixing line (Fig. 5). The Scandinavian shield is also not a relevant sediment source due to missing particle pathways although the presence of chalk fragments in Fram Strait sediments west of Svalbard show the possibility of northward sediment transport by ice rafting from Cretaceaous outcrops as far south as the North Sea area during glacial times (Spielhagen, 1991; Elverhøi et al., 1995). However, this kind of transport was rare.

Input of mantle-derived Sr and Nd is not sig-

nificant in the Arctic Ocean, due to the exceptionally slow spreading rate (1–3 mm a^{-1}) of the Nansen-Gakkel Ridge (Fig. 1b), that results in reduced ocean-floor volcanogenic and hydrothermal activity. There are also no subduction zones and/or volcanic arcs exposed to weathering in the circum-Arctic region, which could contribute mantle-derived material to the Arctic sediments. Therefore, the extended Permo-Triassic flood basalts of the Putorana plateau (Fig. 1a) are the only important exposed source for mantle-derived Sr and Nd ($^{87}Sr/^{86}Sr \sim 0.705$; $\varepsilon_{Nd} \sim 0$; Sharma et al., 1992; Buechel, personal communication) to the eastern Arctic Ocean. The flood basalt weathering products, especially smectite, are found in many marine Arctic sediments and are a good tracer of a Laptev Sea/Kara Sea origin for these sediments (e.g., Wahsner et al., 1999).

5.2.2. Sr and Nd isotopic composition of modern Eurasian shelf and sea ice sediments

The Khatanga and the Yenisey River, drain the flood basalts of the Putorana plateau (Fig. 1a) and basalt weathering products strongly influence the mineralogical and geochemical composition of the shelf and sea ice sediments in the western Laptev Sea (e.g., Behrends et al., 1999; Eisenhauer et al., 1999; Hölemann et al., 1999; Rachold, 1999; Wahsner et al., 1999). The isotopic differences between western Laptev Sea ice samples (average $^{87}Sr/^{86}Sr = 0.714$ and $\varepsilon_{Nd} = -9.0$) and eastern Laptev Sea ice (average $^{87}Sr/^{86}Sr = 0.717$ and $\varepsilon_{Nd} = -12.2$) reflect the isotopic differences among of the Laptev Sea shelf sediments. Eastern Laptev Sea sediments ($^{87}Sr/^{86}Sr = 0.717$, $\varepsilon_{Nd} = -12.5$, Eisenhauer et al., 1999) are dominantly controlled by the Lena river SPM, which has $^{87}Sr/^{86}Sr$ ratios of 0.716 to 0.717 (Rachold et al., 1998; Rachold, 1999). Western Laptev Sea sediments ($^{87}Sr/^{86}Sr = 0.715$; $\varepsilon_{Nd} = -8.7$; Eisenhauer et al., 1999) contain more weathering products from the Siberian flood basalts, especially smectite, and have lower $^{87}Sr/^{86}Sr$ ratios and higher ε_{Nd} values compared to the eastern Laptev Sea. Therefore, the sediments in the sea ice of the Siberian branch of the TPD have a narrow range of isotopic compositions ($^{87}Sr/^{86}Sr = 0.714 \pm 0.001$; $\varepsilon_{Nd} = -9.0 \pm 0.5$) which together with a high contents of smectite and clinopyroxene (Nürnberg et al., 1994; Letzig, 1995; Behrends et al., 1999) indicate an origin from the western Laptev Sea and/or the isotopically and mineralogically indistinguishable material from the eastern Kara Sea shelf (Behrends et al., 1999; Eisenhauer et al., 1999; Wahsner et al., 1999).

Sediment input to the Arctic Ocean by ice rafting from the Kara Sea is of minor importance due to greater water depth and hence less favorable conditions for sediment entrainment by suspension freezing (Pfirman et al., 1997). Therefore, the similarity of the Sr and Nd isotopic compositions of western Laptev Sea surface sediments and sediment-laden sea ice from the Siberian branch of the TPD support the idea that the formation of sediment-laden sea ice by suspension freezing on the western Laptev Sea shelf is a major source for Arctic Ocean sediments (Nürnberg et al., 1994; Eicken et al., 1997). The Sr and Nd isotope compositions of ice rafted shelf sediments trace particle pathways from river-borne Siberian SPM to the open Arctic Ocean by the TPD and can clearly be distinguished from other potential circum-Arctic end-members such as Svalbard, Greenland or Novaya Zemlya (Fig. 5).

5.3. Interglacial sedimentation regime at the Svalbard Margin

During interglacial phases sediment input through sea ice rafting is assumed to dominate the sediment budget to the deep sea of the Arctic Ocean (Clark, 1990; Berner and Wefer, 1990), whereas input of IRD by iceberg rafting is reduced to a minimum.

If sea ice rafting is the most important process of sediment transport, then the Arctic Ocean sediments should have Sr and Nd isotopic compositions similar to those of the Eurasian shelf sediments. However, the average isotopic composition of interglacial core sediments deviates from the characteristic average isotopic composition of modern Arctic Ocean sea ice from the TPD (Table 4, Fig. 5). This indicates an additional input of Svalbard material during interglacial periods, having more radiogenic Sr, but lower ε_{Nd} values. Sr and Nd mixing calculations show that

during MIS 1, 3, and 5 about 75 to 55% of the sediment is delivered by sea ice via the TPD while the 25 to 45% originates from local Svalbard sources (Fig. 5).

5.4. Glacial sedimentation regime at the Svalbard Margin

With the onset of glaciation, increasing amounts of bedrock from the Svalbard archipelago were eroded, because the Svalbard ice sheet extended up to the shelf edge during glacial maxima of MIS 2, 4, 6, and probably also during MIS 5 (Lloyd et al., 1996; Mangerud et al., 1998; Knies et al., 1999) (Fig. 3). Increased iceberg rafting contributed sediment from Svalbard crustal rocks with high $^{87}Sr/^{86}Sr$ ratios and low ε_{Nd} values during the glacier advance. However, the trend of decreasing $^{87}Sr/^{86}Sr$ ratios and increasing ε_{Nd} values in core PS1533 sediments towards the glacial maxima of MIS 2, 4, and 6, especially in termination I and II (Fig. 3) indicates higher input from Eurasian shelf material. This reflects a change in the sediment source from the local Svalbard end-member to increased input from the Eurasian shelf end-member. There are three possible explanations for the increase in Eurasian shelf sediments: (1) intensified ice rafting of shelf sediments by sea ice and/or calving icebergs of the advancing Svalbard/Barents Sea ice sheet; (2) enforced downslope transport by stronger ocean and/or turbidity current activity; and (3) glacial erosion of rocks with isotopic compositions similar to those of the Eurasian shelf sediments.

Possibility 1, ice(-berg) rafting, best explains the observed changes in isotopic, mineralogic and sedimentologic features of the core sediments. Sediment input by sea ice rafting during glacial periods was of minor importance due to the eustatic drop in sea level ($\sim$120 m; Fairbanks, 1989) and shelf exposure. Eurasian shelf areas fell dry, which shifted the loci of sea ice formation towards the Arctic Ocean and decreased suspension freezing into sea ice. Hence, the production of sediment-laden sea ice in the Laptev Sea/Kara Sea area was drastically reduced and sea ice rafting cannot account for the isotopic shift towards the Eurasian shelf end-member. Furthermore, the composition of the Arctic ice cover (i.e. iceberg/sea ice ratio) changed. A greater percentage of icebergs was released from the circum-Arctic ice sheets of Scandinavia, North America, Greenland, and the Barents/Kara Sea in response to extended glaciation of the surrounding continents (e.g., CLIMAP Project Members, 1981; Stein et al., 1994c) and iceberg transport of sediment became more important. We assume that during the last glacial maximum, the sediment flux from Eurasian shelf areas was reduced due to shelf exposure and reduced fluvial run off.

Despite discrepancies between glacial-maximum ice sheet reconstructions the entire Barents Sea area was covered by an ice sheet during the late Weichselian (e.g., Elverhøi et al., 1993; Landvik et al., 1998; Forman et al., 1999; Svendsen et al., 1999). A maximum ice sheet thickness of 2 km was inferred from isostatic crustal response models and postglacial emergence, which indicate maximum ice sheet loading over the central Barents Sea and eastern Svalbard (Lambeck, 1995; Peltier, 1996). Increased influx of warm Atlantic water with the West Spitsbergen Current via the Fram Strait resulted in seasonally open-water conditions as far north as the Yermak Plateau (Vogt et al., 2001) and had an important influence on the moisture supply, triggering the build-up of the SBIS (cf. Hebbeln et al., 1994). The upper Weichselian build-up of the northwestern SBIS was a two-step process between 27 and 23 ka and 19 and 16 ka (Hebbeln et al., 1994; Elverhøi et al., 1995). This correlates well with the fluctuations of the Sr and Nd isotopic composition in MIS 2, which show peaks of Svalbard material during these two build-up phases of the SBIS in core sample 1-5 ($\sim$17.2 ka) and sample 1-8 ($\sim$23.2 ka) (Fig. 3). The stability of this shelf-based ice sheet was strongly controlled by moisture supply and sea level changes (Hebbeln et al., 1994). Hence ice recession took place by rapid calving during sea level rise. During MIS 2 the decay of the SBIS started at 14.5 ka BP (Hebbeln et al., 1994; Elverhøi et al., 1995), which was followed by a second melting event around 13 ka (Nørgaard-Pedersen et al., 1998) that resulted in a rapid retreat of the western SBIS glaciers between 13 and 12 ka (Mangerud et al., 1998) and

a complete break-down of the SBIS after 10 ka. Great amounts of icebergs and melt water spikes were released to the Arctic Ocean during the meltdown of the SBIS and caused IRD peaks and low $\delta^{18}O$ values of foraminifera in the marine record around Svalbard (Stein et al., 1994b; Elverhøi et al., 1995; Lloyd et al., 1996; Vogt et al., 2001). According to our Sr and Nd isotopic data the shelf sediment input reached a maximum during glacial terminations I and II in good agreement with a Laptev/Kara Sea shelf sediment related smectite peak in termination I sediments of the neighboring core PS 2212-3 from Yermak Plateau (Vogt et al., 2001). The isotopic shift towards the Eurasian shelf sediment end-member during terminations I and II, is probably caused by rapid disintegration of the shelf-based SBIS. Especially the meltdown of the northern SBIS margin in the Barents/Kara Sea caused the release of a great number of icebergs with high contents of IRD (incorporated shelf material). This IRD is responsible for the high input of sediment with an isotopic composition of Laptev Sea/Kara Sea material that correlates well with high sand contents (Table 4) in glacial termination core sediments (Fig. 4). There is also evidence for an ice sheet covering the Kara Sea shelf, especially in MIS 4 (Svendsen et al., 1999), which might have contributed such shelf sediments. Furthermore, there was an extensive shelf sediment reworking because of the melt water release and the flooding of the western Siberian shelves due to the contemporaneous sea level rise (cf. Forman et al., 1999). After termination and the Holocene flooding of the Laptev Sea shelf there was a return to the modern interglacial sedimentation regime, which resulted in a rapid increase of $^{87}Sr/^{86}Sr$ ratios and a drop of ε_{Nd} values towards core average values in the Holocene (Fig. 3). According to similar changes of the Sr and Nd isotopic composition in termination II (Fig. 3), a scenario as described above can be assumed also for the penultimate glacial–interglacial cycle.

With regard to point 2, little is known about ocean current activity at the Svalbard Margin and its sediment transport capacity. In general, bottom currents can make large contributions to the clay and silt fraction of marine sediments (e.g., Revel et al., 1996a; Innocent et al., 1997). For example, the formation of a cold and dense nepheloid layer in front of the Barents Sea ice sheet and the release of turbid plumes of subglacial melt water may have been possible (Elverhøi et al., 1993). Although this transport mechanism cannot account for the high IRD content, it may have contributed to the sediment fine fraction. Since the core location is on a submarine swell of the Yermak Plateau, it excludes strong turbidity currents as a major transport process.

For point 3, the contribution of material from another sediment source with similar isotopic composition as Eurasian shelf sediments is considered unlikely because the other potential source terranes have distinct isotopic compositions different from those of Eurasian shelf sediments. Because there is a lack of isotopic data from Barents shelf bedrocks, they cannot be excluded as source for IRD, since the Barents shelf was covered by the SBIS. The Barents shelf itself consists dominantly of Late Triassic to Early Cretaceous sedimentary rocks (coal-bearing sandstones with interbedded shales and carbonates) and some Tertiary sandstones and volcanic rocks in the northern and north-western part, overlain by a thin Quaternary sediment cover (Vorren et al., 1993). During glaciation there has been a supply of Barents Sea shelf bedrock material as IRD to Arctic sediments as indicated by detrital Mesozoic carbonates (e.g., Elverhøi et al., 1995; Vogt, 1997). Such material has not been found in core PS1533 though.

Therefore low $^{87}Sr/^{86}Sr$ ratios and high ε_{Nd} values, high IRD content and low $\delta^{18}O$ values of foraminifera in glacial sediments at the Svalbard Margin most likely originate from melting events of the SBIS and the Kara Sea ice sheet which delivered spikes of reworked Eurasian shelf sediments and fresh water into the Arctic Ocean. Ice-(-berg) rafting is the most likely transport mechanism supplying these sediments.

5.5. Sediment mixing due to glacial–interglacial changes in ice rafting

During a glacial–interglacial cycle, the Sr and

Nd isotopic compositions of core sediments change in a characteristic pattern that is correlated with the extension of the SBIS (Fig. 3). Both Nd and Sr isotopic composition of the core PS1533 sediments record interglacial–glacial shifts that we interpret to reflect changes in sediment provenance due to the erosion of different rock types during advance and retreat of the glaciers from Svalbard onto the Barents Sea shelf. Isotopic data for core samples lie on a mixing hyperbola linking two end-members: Eurasian shelf sediments (A) and Svalbard bedrock (B) (Fig. 5).

With a two-component mixing model, a preliminary quantification of the contributions of both end-members to the core sediments can be made. Mixing proportions were calculated with weighted average Sr and Nd isotopic compositions and concentrations for Eurasian shelf sediments and Svalbard bedrocks (Table 4) using the following mixing equations according to Faure (2001) for the isotopic ratios and elemental concentrations of Sr and Nd in the mixture:

$$[c]_M = [c]_A \times f_A + [c]_B \times (1-f_A) \quad (1)$$

$$(X)_M = (X)_A \times f_A \times \left(\frac{[c]_A}{[c]_M}\right) + (X)_B \times (1-f_A)\frac{[c]_B}{[c]_M} \quad (2)$$

where $[c]_M$ is the element concentration in the mixture; $[c]_A$ is the element concentration in component A; $[c]_B$ is the element concentration in component B; $(X)_M$ is the isotopic ratio of the element in the mixture; $(X)_A$ is the isotopic ratio of the element in component A; $(X)_B$ is the isotopic ratio of the element in component B; and f_A mixing parameter giving the abundance of component A in the mixture.

Mixing calculations were made with two assumptions: (a) the Sr and Nd isotopic composition of Eurasian shelf sediments, which ultimately reflect the fluvial input supplied to the Arctic Ocean, did not change significantly during the last 140 ka; and (b) the isotopic composition of crystalline bedrocks from Svalbard is representative for the sedimentary input from Svalbard. Svalbard is the most likely isotopic end-member for material from old continental crust with low ε_{Nd} values and high $^{87}Sr/^{86}Sr$ ratios. Sr and Nd isotope data for shelf sediments are available only for modern SPM and surface sediments (Rachold et al., 1998; Eisenhauer et al., 1999; this study). The isotopic composition of Eurasian shelf sediments and hence TPD sea ice sediments may have varied with time due to changing hinterland erosion, fluvial activity and sea level, but this is unknown and hence, cannot be considered in the mixing calculations.

According to the mixing calculations, average core PS1533 Sr and Nd isotopic compositions (Table 4) represent a mixture of ~70% Eurasian shelf sediments and ~30% Svalbard-derived material (Fig. 5). Eurasian shelf sediment contribution to core sediments varies between the 30 and 95% while local input of Svalbard material accounts for 70 to 5%. During waxing of the Svalbard glaciers the input of the Svalbard material increases by a factor of two compared to average interglacial core sediments. This shift to more input from Svalbard material (up to 70%) during build-up of the SBIS is caused by advancing Svalbard glaciers (Elverhøi et al., 1995; Lloyd et al., 1996; Mangerud et al., 1998) and intensified glacial erosion and supply of material from the Precambrian/Palaeozoic bedrock by icebergs. Towards the glacial maxima in MIS 2, 4 and 6 higher ε_{Nd} values indicate an increase in shelf sediment input, due to increased glacial erosion and ice rafting of shelf sediments during SBIS extension onto the Barents Sea shelf. In termination I and II there is a sharp increase to highest ε_{Nd} values and a decrease to lowest $^{87}Sr/^{86}Sr$ ratios in the core (Fig. 3) similar to values of modern shelf and sea ice sediment (Fig. 5) which were probably caused by shelf sediment spikes resulting from intense iceberg rafting during rapid decay of the shelf-based SBIS and shelf sediment reworking during flooding of the Eurasian shelves. In these IRD-rich sediments Eurasian shelf material contribute up to 95% of the < 63 μm fraction and Svalbard material decreases to a minimum of 5–10% (Fig. 5).

6. Conclusions

The $^{87}Sr/^{86}Sr$ ratio alone is an ambiguous tracer of sediment provenance, because it can vary due to grain-size effects despite sediment derivation from the same source. In contrast, size fractions from the same crustal source have similar ε_{Nd} values. Therefore, differences in Sm–Nd isotopic compositions of clay- and silt-size fractions are clearly related to different crustal sources. This may allow for a reconstruction of particle provenance and transport processes supplying different size fractions in deep-sea sediments.

The Sr and Nd isotopic composition of core PS1533 sediments show large temporal variations that follow systematic glacial–interglacial cycles. These reflect the growth and decay of the SBIS resulting in changes of the sediment sources, which coincide with changes of sediment transport mechanisms from sea ice to icebergs. The variations are interpreted as mixtures of Eurasian shelf sediment and Svalbard bedrock material with mixing proportions of both end-members varying in response to glacial–interglacial oscillations of ice sheet extension and sedimentation regime of the Arctic Ocean. During build-up phases of the SBIS, input of Svalbard material reached maximum values due to intensified glacial erosion of the Proterozoic/Palaeozoic bedrocks when glaciers advanced from Svalbard fjords onto the Barents Sea shelf. In contrast, during maximum extensions of the SBIS up to the shelf edge and ice sheet breakdown of the northern SBIS margin and/or the Kara Sea ice sheet, increasing amounts of Eurasian shelf sediments were supplied by iceberg rafting and shelf sediment reworking, especially during glacial termination I and II.

The Sr and Nd isotopic composition of modern Arctic sea ice and shelf sediments confirm sea ice rafting as a dominant transport mechanism for Eurasian shelf sediments to the Arctic Ocean. Modern sediment-laden sea ice of the Siberian branch of the TPD has an isotopic composition similar to that of the Eurasian shelf source areas, especially to those of the western Laptev and Kara Sea. Similar Sr and Nd isotopic composition as Eurasian shelf sediments in termination I and II core sediments reflect shelf sediment spikes during deglaciation events of the nearby shelf-based SBIS. Hence, Sr and Nd isotopic composition of marine Arctic sediments can be used as a tracer of continental glaciation and ice rafting.

Acknowledgements

We thank D. Dethleff for providing the sea ice and shelf sediment samples and R. Spielhagen for the samples of sediment core PS1533. Further we are grateful for the partly unpublished Sr and Nd data from Svalbard rocks that were kindly supplied by Å. Johansson. We also thank T. Vennemann, C. Vogt and J. O'Neil for helpful comments and discussions. This manuscript further benefitted from thoughtful and detailed reviews of Clark Johnsen and Christophe Innocent. This study was funded by the Deutsche Forschungsgemeinschaft (DFG), Grant Ei 272/5-1.

References

Aagaard, K., Carmack, E.C., 1989. The role of sea ice and fresh water in the arctic circulation. J. Geophys. Res. 94, 14485–14498.

Aagaard, K., Carmack, E.C., 1994. The Arctic Ocean and climate: a perspective. In: Johannessen, O.M., Muench, R.D., Overland, J.E. (Eds.), The Polar Oceans and Their Role in Shaping the Global Environment: The Nansen Centennial Volume. American Geophysical Union, Washington, DC, Geophysical Monograph, pp. 5–20.

Alley, R.B., 1995. Resolved: The Arctic controls global climate change. In: Smith W.O. Jr., Grebmeier, J.M. (Eds.), Arctic Oceanography: Marginal Ice Zones and Continental Shelves. American Geophysical Union, Washington DC, Costal and Estuarine Studies, pp. 263–284.

Anderson, L.G., Björk, G., Holby, O., Jones, E.P., Kattner, G., Koltermann, K.P., Liljeblad, B., Lindegren, R., Rudels, B., Swift, J., 1994. Water masses and circulation in the Eurasian basin: Results from the Oden 91 North pole expedition. J. Geophys. Res. 99, 3273–3283.

Asahara, Y., Tanaka, T., Kamioka, H., Nishimura, A., 1995. Asian continental nature of $^{87}Sr/^{86}Sr$ ratios in north central Pacific sediments. Earth Planet. Sci. Lett. 133, 105–116.

Behrends, M., Hoops, E., Peregovich, B., 1999. Distribution patterns of heavy minerals in Siberian rivers, the Laptev Sea and the Eastern Arctic Ocean: an approach to identify sources, transport and pathways of terrigenous matter. In: Kassens, H., Bauch, H.A., Dmitrenko, I.A., Eicken, H., Hub-

berten, H.-W., Melles, M., Thiede, J., Timokhov, L.A. (Eds.), Land–Ocean Systems in the Siberian Arctic, Dynamics and History. Springer, New York, pp. 265–286.

Berner, H., Wefer, G., 1990. Physiographic and biologic factors controlling surface sediment distribution in the Fram Strait. In: Bleil, U., Thiede, J. (Eds.), Geological History of the Polar Oceans: Arctic versus Antarctic. NATO ASI Series C 308, pp. 317–335.

Bischof, J., Koch, J., Kubisch, M., Spielhagen, R.F., Tiede, J., 1990. Nordic Seas surface ice drift reconstructions: evidence from ice rafted coal fragments during oxygen isotope stage 6. In: Dowdeswell, J.A., Scourse, J.D. (Eds.), Glacimarine Environments: Processes and Sediments. Geol. Soc. Spec. Publ. 53, pp. 235–251.

Bischof, J., Clark, D.L., Vincent, J.S., 1996. Origin of ice-rafted debris: Pleistocene paleoceanography in the western Arctic Ocean. Paleoceanography 11, 757–772.

Clark, D.L., 1990. Arctic Ocean ice cover; geologic history and climatic significance. In: Grantz, A., Johnson, L., Sweeney, J.F. (Eds.), The Arctic Ocean Region. (The Geology of North America). Geol. Soc. Am., Boulder, CO, pp. 53–62.

CLIMAP Project Members, 1981. Maps of northern and southern hemisphere continental ice, sea ice, and sea surface temperatures in August for the modern and the last glacial maximum. Geol. Soc., Map and Chart Series. MC-36, maps 7A and 7B.

Colony, R., Thorndyke, A.S., 1985. An estimate of the mean field of Arctic sea-ice motion. J. Geophys. Res. C1, 965–974.

Dasch, E., 1969. Strontium isotopes in weathering profiles, deep sea sediments and sedimentary rocks. Geochim. Cosmochim. Acta 33, 1521–1552.

Douglas, G.B., Gray, C.M., Hart, B.T., Beckett, R., 1995. A strontium isotopic investigation of the origin of suspended particulate matter (SPM) in the Murray-Darling River system, Australia. Geochim. Cosmochim. Acta 59, 3799–3815.

Eicken, H., Reimnitz, E., Alexandrov, T., Martin, T., Kassens, H., Viehoff, T., 1997. Sea-ice export processes in the Laptev Sea and their importance for sediment export. Cont. Shelf Res. 17, 205–233.

Eisenhauer, A., Spielhagen, R.F., Frank, M., Hentzschel, G., Mangini, A., Kubik, W., Dittrich-Hannen, B., Billen, T., 1994. ^{10}Be records of sediment cores from high northern latitudes: Implications for environmental and climatic changes. Earth Planet. Sci. Lett. 124, 171–184.

Eisenhauer, A., Meyer, H., Rachold, V., Tütken, T., Wiegand, B., Hansen, B.T., Spielhagen, R.F., Lindemann, F., Kassens, H., 1999. Grain-size separation and sediment mixing in Arctic Ocean sediments: evidence from strontium isotope systematic. Chem. Geol. 158, 173–188.

Elverhøi, A., Fjeldskaar, W., Solheim, A., Nyland-Berg, M., Russwurm, L., 1993. The Barents Sea ice sheet – a model of its growth and decay during the last ice maximum. Quat. Sci. Rev. 12, 863–873.

Elverhøi, A., Andersen, E.S., Dokken, T., Hebbeln, D., Spielhagen, R., Svedsen, J.I., Sorflaten, M., Rornes, A., Hald, M., Forsberg, C.F., 1995. The growth and decay of the late Weichselian ice sheet in western Svalbard and adjacent areas based on Provenance studies of marine Sediments. Quat. Res. 44, 303–316.

Fagel, N., Innocent, C., Stevenson, R.K., Hillaire-Marcel, C., 1999. Deep circulation changes in the Labrador Sea since the last glacial maximum; new constraints from Sm–Nd data on sediments. Paleoceanography 14, 777–788.

Fahl, K., Stein, R., 1999. Biomarkers as organic-carbon-source and environmental indicators in the late Quaternary Arctic Ocean; problems and perspectives. Mar. Chem. 63, 293–309.

Fairbanks, R.G., 1989. A 17.000-year glacio-eustatic sea level record: influence of glacial melting rates on the Younger Dryas event and deep ocean circulation. Nature 342, 637–642.

Faure, G., 2001. Origin of Igneous Rocks – The Isotopic evidence. Springer, Berlin, pp. 496.

Forman, S.L., Ingólfsson, Ó., Gataullin, V., Manley, F.W., Lokrantz, H., 1999. Late Quaternary stratigraphy of western Yamal Peninsula, Russia: New constraints on the configuration of the Eurasian ice sheet. Geology 27, 807–810.

Gee, D.G., Björklund, L., Stölen, L.-K., 1994. Early Proterozoic basement in Ny Friesland – implications for the Caledonian tectonics of Svalbard. Tectonophysics 231, 171–182.

Gee, D.G., Johansson, Å., Ohta, Y., Tebenkov, A.M., Krasil'scikov, A.A., Balashov, Yu.A., Larionov, A.N., Gannibal, L.F., Ryungenen, G.I., 1995. Grenvillian basement and a major unconformity within the Caledonides of Nordaustlandet Svalbard. Precambrian Res. 70, 215–234.

Goldstein, S.J., Jacobsen, S.B., 1988. Nd and Sr isotopic systematics of river water suspended material: implications for crustal evolution. Earth Planet. Sci. Lett. 87, 249–265.

Goldstein, S.L., O'Nions, R.K., 1981. Nd and Sr isotopic relationship in pelagic clays and ferromanganese deposits. Nature 292, 324–327.

Goldstein, S.L., O'Nions, R.K., Hamilton, J., 1984. A Sm–Nd isotopic study of atmospheric dusts and particulates from major river systems. Earth Planet. Sci. Lett. 70, 221–236.

Gordeev, V.V., Martin, J.M., Siderov, I.S., Siderova, M.V., 1996. A reassessment of the Eurasian river input of water, sediment, major elements and nutrients to the Arctic Ocean. Am. J. Sci. 296, 664–691.

Gordienko, A., Laktionov, A.F., 1969. Circulation and physics of the Arctic basin waters. In: Gordonand, A.L., Baker, F.W.G. (Eds.), Ann. Int. Geophys. Year. Oceanography, 46, Pergamon, New York, pp. 94–112.

Grousset, F.E., Biscaye, P.E., Zindler, A., Prospero, J., Chester, R., 1988. Nd isotopes as tracers in marine sediments and aerosols: North Atlantic. Earth Planet. Sci. Lett. 87, 367–378.

Grousset, F.E., Biscaye, P.E., Revel, M., Petit, J.R., Pye, K., Joussaume, S., Jouzel, J., 1992. Antarctic (Dome C) ice-core dust at 18 k.y. B.P.: isotopic constraints on origins. Earth Planet. Sci. Lett. 111, 175–182.

Harland, W.B., 1985. Caledonide Svalbard. In: Gee, D.G., Sturt, B.A. (Eds.), The Caledonide Orogen – Scandinavia and Related Areas. Wiley, Chichester, pp. 991–1016.

Hebbeln, D., Wefer, 1991. Effects of ice-cover and ice-rafted

material on sedimentation in the Fram Strait. Nature 350, 409–411.

Hebbeln, D., Dokken, T., Andersen, E.S., Hald, M., Elverhøi, A., 1994. Moisture supply for northern ice sheet growth during the Last Glacial Maximum. Nature 370, 357–359.

Hemming, S.R., Broecker, W.S., Sharp, W.D., Bond, G.C., Gwiazda, R.H., McManus, J.F., Klas, M., Hajdas, I., 1998. Provenance of Heinrich layers in core V28-82, northeastern Atlantic: $^{40}Ar/^{39}Ar$ ages of ice-rafted hornblende, Pb isotopes in feldspar grains, and Nd–Sr–Pb isotopes in the fine sediment fraction. Earth Planet. Sci. Lett. 164, 317–333.

Hölemann, J.A., Schirmacher, M., Prange, A., 1999. Dissolved and particulate major and trace elements in newly formed ice from the Laptev Sea. In: Kassens, H., Bauch, H.A., Dmitrenko, I.A., Eicken, H., Hubberten, H.-W., Melles, M., Thiede, J., Timokhov, L.A. (Eds.), Land–Ocean Systems in the Siberian Arctic, Dynamics and History. Springer, New York, pp. 101–111.

Imbrie, J., Hays, J.D., Martinson, D.G., McIntyre, A., Mix, A.C., Morley, J.J., Pisias, N.G., Prell, W.L., Shackleton, N.J., 1984. The orbital theory of Pleistocene climate: Support from a revised chronology of the marine $\delta^{18}O$ record. In: Berger, A.L. et al. (Eds.), Milankovtich and Climate. Kluwer, Dordrecht, pp. 269–305.

Innocent, C., Fagel, N., Stevenson, R.K., Hillaire-Marcel, C., 1997. Sm–Nd signature of modern and late Quaternary sediments from the northwest North Atlantic: Implications for deep current changes since the Last Glacial Maximum. Earth Planet. Sci. Lett. 146, 607–625.

Innocent, C., Fagel, N., Hillaire-Marcel, C., 2000. Sm–Nd isotope systematics in deep-sea sediments: clay-size versus coarser fractions. Mar. Geol. 168, 79–87.

Jacobsen, S.B., Wasserburg, G.J., 1980. Sm–Nd isotopic evolution of chondrites. Earth Planet. Sci. Lett. 50, 139–155.

Johansson, Å., Gee, D.G., 1999. The late Palaeoproterozoic Eskolabreen granitoids of southern Ny Friesland, Svalbard Caledonides – geochemistry, age and origin. GFF 121, 113–126.

Johansson, Å., Gee, D.G., Björklund, L., Witt-Nilsson, P., 1995. Isotope studies of granitoids from Bangenhuk Formation, Ny Friesland Caledonides. Svalbard. Geol. Mag. 132, 303–320.

Johansson, Å., Larionov, A.N., Tebenkov, A.M., Gee, D.G., Whitehouse, M.J., Vestin, J., 2000. Grenvillian magmatism of western and central Nordaustlandet, northeastern Svalbard. Trans. R. Soc. Edinburgh: Earth Sci. 90, 221–254.

Knies, J., Vogt, C., Stein, R., 1999. Late Quaternary growth and decay of the Svalbard/Barents Sea ice sheet and paleoceanographic evolution of the adjacent Arctic Ocean. Geomar. Lett. 18, 195–202.

Knies, J., Nowaczyk, N., Müller, C., Vogt, C., Stein, R., 2000. A multiproxy approach to reconstruct the environmental changes along the Eurasian continental margin over the last 150.000 years. Mar. Geol. 163, 317–344.

Kubisch, M., 1992. Die Eisdrift im Arktischen Ozean während der letzten 250.000 Jahre. GEOMAR Report, 16, Kiel, pp. 1–100.

Lambeck, K., 1995. Constraints on the Late Weichselian ice sheet over the Barents Sea from observations of raised shorelines. Quat. Sci. Rev. 14, 1–16.

Landvik, J.K., Bondevik, S., Elverhøi, A., Fjeldskaar, W., Mangerud, J., Siegert, M.J., Salvigsen, O., Svendsen, J.-I., Vorren, T.O., 1998. The last glacial maximum of Svalbard and the Barents Sea area: Ice sheet extent and configuration. Quat. Sci. Rev. 17, 43–75.

Letzig, T., 1995. Sea ice-transported lithogenic fine fraction of Late Quaternary deep-sea sediments of the central eastern Arctic Ocean and the Fram Strait. Rep. Pol. Res. 162, 98.

Lloyd, J.M., Kroon, D., Boulton, G.S., Laban, C., Fallick, A., 1996. Ice rafting history from the Spitsbergen ice cap over the last 200-kyr. Mar. Geol. 131, 103–121.

Mangerud, J., Dokken, T., Hebbeln, D., Heggen, B., Ingólfsson, Ó., Landvik, J.I., Mejdahl, V., Svendsen, J.I., Vorren, T.O., 1998. Fluctuations of Svalbard Barents Sea Ice Sheet during the last 150.000 years. Quat. Sci. Rev. 17, 11–42.

McCulloch, M.T., Wasserburg, G.J., 1978. Sm–Nd and Rb–Sr chronology of continental crust formation. Science 200, 1003–1011.

McLennan, S.M., McCulloch, M.T., Taylor, S.R., Maynard, J.B., 1989. Effects of sedimentary sorting on neodymium isotopes in deep sea turbidites. Nature 337, 547–549.

Miller, R.G., O'Nions, R.K., Hamilton, J., Welin, E., 1986. Crustal residence ages of clastic sediments, orogeny and continental evolution. Chem. Geol. 57, 87–99.

Milliman, J.D., Meade, R.H., 1983. World-wide delivery of river sediment to the oceans. J. Geol. 91, 1–21.

Nørgaard-Pedersen, N.R., Spielhagen, R.F., Thiede, J., Kassens, H., 1998. Central Arctic Ocean environment during the last 80.000 years. Paleoceanography 12, 193–204.

Nürnberg, D., Wollenburg, I., Dethleff, D., Eicken, H., Kassens, H., Letzig, T., Reimnitz, E., Thiede, J., 1994. Sediments in Arctic sea ice – implications for entrainment transport and release. Mar. Geol. 119, 185–214.

Peltier, W.R., 1996. Mantle viscosity and ice-age ice sheet topography. Science 273, 1359–1363.

Pfirman, S.L., Colony, R., Nürnberg, D., Eicken, H., Rigor, I., 1997. Reconstructing the origin and trajectory of drifting Arctic sea ice. J. Geophys. Res. 102, 12575–12586.

Rachold, V., 1999. Major, trace, rare earth element geochemistry of suspended particulate material of east Siberian rivers draining to the Arctic Ocean. In: Kassens, H., Bauch, H.A., Dmitrenko, I.A., Eicken, H., Hubberten, H.-W., Melles, M., Thiede, J., Timokhov, L.A. (Eds.), Land–Ocean Systems in the Siberian Arctic, Dynamics and History. Springer, New York, pp. 199–222.

Rachold, V., Eisenhauer, A., Hubberten, H.-W., Hansen, B.T., Meyer, H., 1998. Sr Isotope composition of suspended particulate material (SPM) of East Siberian rivers: sediment transport to the Arctic Ocean. Arct. Alp. Res. 4, 422–429.

Revel, M., Cremer, M., Grousset, F.E., Labeyrie, L., 1996a. Grain-size and Sr–Nd isotopes as tracer of palaeo-bottom

current strength, Northeast Atlantic Ocean. Mar. Geol. 131, 233–249.

Revel, M., Sinko, J.A., Grousset, F.E., 1996b. Sr and Nd isotopes as tracers of North Atlantic lithic particles: Palaeoclimatic implications. Palaeogeogr. Palaeoclimatol. Palaeoecol. 11, 95–113.

Reimnitz, E., Dethleff, D., Nürnberg, D., 1994. Contrasts in Arctic shelf sea-ice regimes and some implications: Beaufort Sea versus Laptev Sea. Mar. Geol. 119, 215–225.

Schubert, C.J., Stein, R., 1996. Deposition of organic carbon in late Quaternary Arctic Ocean: terrigenous supply vs. marine productivity. Org. Geochem. 24, 421–436.

Sharma, M., Basu-Asish, R., Nesterenko, G.V., 1992. Temporal Sr-, Nd-, and Pb-isotopic variations in the Siberian flood basalts, implications for the plume-source characteristics. Earth Planet. Sci. Lett. 113, 365–381.

Spielhagen, R., 1991. Die Eisdrift der Framstrasse während der letzten 200.000 Jahre. Dissertation. GEOMAR Report, 4, Kiel, pp. 1–144.

Spielhagen, R., Erlenkeuser, H., 1994. Stable oxygen and carbon isotopes in planktic foraminifers from Arctic Ocean surface sediments: Reflection of the total salinity surface water layer. Mar. Geol. 119, 227–250.

Spielhagen, R.F., Bonani, G., Eisenhauer, A., Frank, M., Frederichs, T., Kassens, H., Kubik, W., Mangini, A., Nørgaard-Pedersen, N., Nowaczyk, N.R., Schäper, S., Stein, R., Thiede, J., Thiedemann, R., Wahsner, M., 1997. Arctic Ocean evidence for late Quaternary initiation of northern Eurasian ice sheets. Geology 25, 783–786.

Stein, R., Grobe, H., Wahsner, M., 1994a. Organic carbon, carbonate, and clay mineral distribution in central Arctic Ocean surface sediments. Mar. Geol. 119, 269–285.

Stein, R., Schubert, C., Vogt, C., Fütterer, D., 1994b. Stable isotope stratigraphy, sedimentation rates, and salinity changes in the Latest Pleistocene to Holocene eastern central Arctic Ocean. Mar. Geol. 119, 333–355.

Stein, R., Nam, S.-I., Schubert, C., Vogt, C., Fütterer, D., Heinemeier, J., 1994c. The last deglaciation event in the eastern central Arctic Ocean. Science 264, 692–696.

Svendsen, J.L., Astakhov, V.I., Bolshiyanov, D.Yu., Demidov, I., Dowdeswell, J.A., Gataullin, V., Hjort, C., Hubberten, H.W., Larsen, E., Mangerud, J., Melles, M., Möller, P., Saarnisto, M., Siegert, M.J., 1999. Maximum extent of the Eurasian ice sheets in the Barents and Kara Sea region during the Weichselian. Boreas 28, 234–242.

Velichkov, A.A., Kononov, Y.M., Faustova, A., 1997. The last glaciation of Earth: Size and volume of ice sheets. Quat. Int. 41/42, 43–51.

Vogt, C., 1997. Regional and temporal variations of mineral assemblages in Arctic Ocean sediments as climatic indicator during glacial/interglacial changes. Rep. Pol. Res. 251, 309.

Vogt, C., Knies, J., Spielhagen, R., Stein, R., 2001. Detailed mineralogical evidence for two nearly identical glacial/deglacial cycles and Atlantic Water advection to the Arctic Ocean during the last 90.000 years. Global and Planetary Change 31, 23–44.

Vorren, T.O., Bergsager, E., Dahl-Stamnes, Ø.A., Holter, E.B., Johansen, B., Lie, E., Lund, T.B. (Eds.), 1993. Arctic Geology and Petroleum Potential, Special Publication. Elsevier, Amsterdam, 751 pp.

Wahsner, M., Müller, C., Ivanov, G., Nürnberg, D., Shelekhova, E.S., Stein, R., Tarasov, G., 1999. Clay mineral distributions in surface sediments from the Eurasian Arctic Ocean and the Eurasian continental margin as indicator for source areas and transport pathways of sediments – A synthesis. Boreas 28, 215–233.

Walter, H.J., Hegner, E., Diekmann, B., Kuhn, G., Rutgers van der Loeff, M.M., 2000. Provenance and transport of terrigenous sediment in the south Atlantic Ocean and their relations to glacial and interglacial cycles: Nd and Sr isotopic evidence. Geochim. Cosmochim. Acta 64, 3813–3827.

Weis, D., Demaiffe, D., Souchez, R., Gow, A.J., Meese, D.A., 1997. Ice sheet development in Central Greenland: implications from the Nd, Sr, Pb isotopic compositions of basal material. Earth Planet. Sci. Lett. 150, 161–169.

Winter, B.L., Johnson, C.L., Clark, D.L., 1997. Strontium, neodymium and lead isotope variations of authigenic and silicate sediment components from the Late Cenozoic Arctic Ocean: Implications for sediment provenance and source of trace metals in sea water. Geochim. Cosmochim. Acta 61, 4181–4200.